



Scholars' Mine

Masters Theses


Student Theses and Dissertations

Spring 2019

Routing algorithm for the ground team in transmission line inspection using unmanned aerial vehicle

Yu Li

Follow this and additional works at: https://scholarsmine.mst.edu/masters_theses

 Part of the [Operations Research, Systems Engineering and Industrial Engineering Commons](#), and the [Robotics Commons](#)

Department:

Recommended Citation

Li, Yu, "Routing algorithm for the ground team in transmission line inspection using unmanned aerial vehicle" (2019). *Masters Theses*. 7887.
https://scholarsmine.mst.edu/masters_theses/7887

This thesis is brought to you by Scholars' Mine, a service of the Missouri S&T Library and Learning Resources. This work is protected by U. S. Copyright Law. Unauthorized use including reproduction for redistribution requires the permission of the copyright holder. For more information, please contact scholarsmine@mst.edu.

ROUTING ALGORITHM FOR THE GROUND TEAM IN TRANSMISSION LINE

INSPECTION USING UNMANNED AERIAL VEHICLE

by

YU LI

A THESIS

Presented to the Faculty of the Graduate School of the

MISSOURI UNIVERSITY OF SCIENCE AND TECHNOLOGY

In Partial Fulfillment of the Requirements for the Degree

MASTER OF SCIENCE IN SYSTEMS ENGINEERING

2019

Approved by:

Dr. Zeyi Sun, Advisor

Dr. Ruwen Qin

Dr. Cihan Dagli

© 2019

Yu Li

All Rights Reserved

ABSTRACT

With the rapid development of robotics technology, robots are increasingly used to conduct various tasks by utility companies. An unmanned aerial vehicle (UAV) is an efficient robot that can be used to inspect high-voltage transmission lines. UAVs need to stay within a data transmission range from the ground station and periodically land to replace the battery in order to ensure that the power system can support its operation. A routing algorithm must be used in order to guide the motion and deployment of the ground station while using UAV in transmission line inspection. Most existing routing algorithms are dedicated to pathfinding for a single object that needs to travel from a given start point to end point and cannot be directly used for guiding the ground station deployment and motion since multiple objects (i.e., the UAV and the ground team) whose motions and locations need to be coordinated are involved. In this thesis, we intend to explore the routing algorithm that can be used by utility companies to effectively utilize UAVs in transmission line inspection. Both heuristic and analytical algorithms are proposed to guide the deployment of the ground station and the landing point for UAV power system change. A case study was conducted to validate the effectiveness of the proposed routing algorithm and examine the performance and cost-effectiveness.

ACKNOWLEDGMENTS

I am very grateful to my advisor, Dr. Zeyi Sun, for his unwavering support and belief in me. His advice has led me to the right way. It has been my greatest honor to work with him. He helped me a lot and support throughout my master's study. I am forever grateful to him.

I would like to extend my appreciation to the committee members Dr. Ruwen Qin and Dr. Cihan Dagli for their valuable feedback about this thesis.

I am thankful to Ameren, especially the project advisor, Mr. Lorne Poindexter, as well as Mr. George Mues, for funding this research and providing guidance and various constructive and insightful suggestions to this study.

Finally, I would like to thank my parents, my grandmother, and well-wishers. Without their support, I wouldn't be able to reach this far.

TABLE OF CONTENTS

	Page
ABSTRACT.....	iii
ACKNOWLEDGMENTS	iv
LIST OF ILLUSTRATIONS	vii
LIST OF TABLES	ix
 SECTION	
1. INTRODUCTION.....	1
1.1. BACKGROUND	1
1.2. MOTIVATION.....	4
2. LITERATURE REVIEW.....	6
2.1. UAV TECHNOLOGY APPLICATION	6
2.2. ROUTING ALGORITHMS	7
2.3. ROBOT PATH PLANNING	8
2.4. PARTICLE SWARM OPTIMIZATION	9
3. HEURISTIC MODEL.....	12
3.1. HEURISTIC ROUTING ALGORITHM	12
3.1.1. For the UAV Powered by the Lithium Battery.	13
3.1.2. For the UAV Powered by Hydrogen Fuel Cell.	15
3.2. COST MODEL.....	16
3.2.1. Total Travel Time of the Ground Team.	18
3.2.2. Working Time.	18

3.2.3. Total Setup Time.....	19
3.2.4. Battery Depreciation Cost.....	21
3.2.5. Cell Depreciation Cost.....	24
3.3. CASE STUDY	25
3.4. CONCLUSION.....	34
4. ANALYTICAL MODEL	35
4.1. ANALYTICAL ALGORITHM AND COST MODEL	36
4.2. SOLUTION STRATEGY BASED ON PSO	46
4.3. CASE STUDY	53
4.4. CONCLUSION.....	58
5. CONCLUSIONS	60
BIBLIOGRAPHY	61
VITA.....	69

LIST OF ILLUSTRATIONS

	Page
Figure 1-1. Robot for Transmission Line Inspection.....	3
Figure 3-1. The General Method of the Inspection.....	14
Figure 3-2. Fuel Tank Replacement.....	21
Figure 3-3. Lithium Battery Power System and Cost Components.....	21
Figure 3-4. Lithium Battery Recharging Illustration	22
Figure 3-5. Hydrogen Fuel Cell Power System and Cost Components.....	24
Figure 3-6. Cost Decrement Chart of the Suspended Robot and UAV	34
Figure 4-1. The Analytical General Method of the Inspection	37
Figure 4-2. Ground Station Deployment & Relocation Scenario 1	38
Figure 4-3. Ground Station Deployment & Relocation Scenario 2	39
Figure 4-4. Ground Station Deployment & Relocation Scenario 3	39
Figure 4-5. Virtual Points	43
Figure 4-6. Particle Dimension Reduction Example	48
Figure 4-7. Flowchart of the Analytical Algorithm	52
Figure 4-8. Parameters of PSO Algorithm.....	53
Figure 4-9. Deployment and Replacement Comparison of 38km	54
Figure 4-10. Deployment and Replacement Comparison of 50km	55
Figure 4-11. Comparison of Unit Time	56
Figure 4-12. Comparison of Unit Cost	56

Figure 4-13. Comparison of Unit Salary Cost	57
Figure 4-14. Comparison of Unit Setup Cost	58
Figure 4-15. Comparison of Unit Battery/Cell Depreciation Cost	58

LIST OF TABLES

	Page
Table 3-1. Cost Component and Formulation.....	17
Table 3-2. The Result of Total Time for the Inspection and the Salary Cost	29
Table 3-3. Parameters for Equipment Involved in Operation.....	29
Table 3-4. Total Cost of UAV for inspection	33
Table 3-5. Cost Decrement Table of the Suspended Robot and UAV	33
Table 4-1. Comparison Result of Two Method	54

1. INTRODUCTION

1.1. BACKGROUND

High-voltage transmission line systems play a critical role in building a reliable energy supply infrastructure in the country. In particular, with the fast growth of the penetration of renewable sources in electricity grid in recent years (Bastian and Trainor, 2010; Wang et al., 2010; Yaqub et al., 2012), the transmission line system becomes even more critical to deliver the energy with low environmental burden to end-use customers. Transmission lines in the power system are subject to usage deterioration and environmental corrosion. To ensure a highly reliable energy supply system, the reliability of the transmission line system itself needs to be intensively monitored and carefully maintained so that the health of the system can be determined and possible issues such as material degradation, environmental corruptions, etc., can be timely detected. A great deal of research focusing on reliability modeling and maintenance strategy for the transmission system as well as other critical infrastructures has been reported (Ge, 2010; Mahmoudi et al., 2014; Wilmeth and Usrey, 2000).

Traditionally, regular inspection of transmission line is conducted with the aid of helicopters by linemen using hot sticks (Whitworth et al., 2001; Yan et al., 2007; Earp et al., 2011) at heights of several hundred feet (Roncolato et al., 2010). Sometimes, if required, linemen need to walk on the transmission line to implement inspection tasks. Such a “manual” inspection mode is highly sensitive to undesirable weather conditions (Roncolato et al., 2010). The inspection progress is severely limited by the workload limit of human beings, and thus the inspection is typically very time-consuming. In

addition, worker safety, which is considered one of the most fundamental indicators of a company's social sustainability (Pagell et al., 2014), is one of the primary concern of this job; therefore, the linemen need to be intensively trained so that they can be safe in such a dangerous working environment both physically and psychologically. Moreover, the cost and energy consumption involved when employing a helicopter is fairly high, which further exacerbates the sustainability concerns of practitioners, communities, government agencies, and society as a whole.

To address such sustainability concerns, many utility companies have begun to seek out emerging smart technologies that can be used to replace linemen in transmission line inspection. One promising technology that has drawn wide interest from utility companies is robot technology.

Robot technology is not novel in practice. For example, many studies focusing on the utilization of robotic technology in manufacturing have been reported. The attitudes toward the introduction of robots in a unionized automobile environment were studied in 1995 by Herold et al.. A survey was conducted to evaluate the role and future of robot technology in Australian manufacturing, which included general manufacturing, automotive, plastics molding, and electronics industries (Orr, 1996). The flexibility of a vision-based robot used in a manufacturing environment was enhanced using an artificial neural network approach (Sim and Teo, 1997). A benefit of industrial robotics into a lean manufacturing system was investigated (Hedelind and Jackson, 2011). Furthermore, robot technology has been effectively applied in the inspection of various complex systems, such as underwater system (Asakawa et al., 2012) and tunnel system (Yao et al., 2003).

Since the last decade, literature regarding the application of robots in transmission line inspection has been reported (Montambault and Pouliot, 2003; Montambault and Pouliot, 2004; Laugier and Siegwart, 2008). Generally, three major types of robots, i.e., land-based (Quanta Technology, 2015), suspended-based, and aerial-based (ULC Robotics, 2018) robots as shown in Figure 1-1, have been designed and developed for applications in the power transmission sector (Elizondo et al., 2010). The land-based robot is usually placed on by boom trucks on the ground and remotely controlled by the radio (Elizondo et al., 2010). They used for replacing insulators and conducting other heavy-duty tasks such as providing temporary support to conductors in the absence of a steel structure as shown in Figure 1-1a (Elizondo et al., 2010). The suspended-based robot is suspended from the conductor lines via wheels that facilitate the movement of the robot and is used for inspecting conductor lines and performing minor (Elizondo et al., 2010). The aerial-based robot is typically an unmanned aerial vehicle (UAV) as shown in Figure 1-1b and is used for inspecting the state of the conductor (Elizondo et al., 2010). It is controlled by radios with a geographical position system.



a. Land based robot



b. Aerial based robot



c. Suspended based robot

Figure 1-1. Robot for Transmission Line Inspection

In general, the land-based robot technology is the most mature, and thus it has been widely used in the power industry. Both the suspended-based robot and unmanned aerial vehicle (UAV) have passed onsite testing with a full load and have been commercialized for a few years.

1.2. MOTIVATION

Today, the study of adopting robots for use in transmission line inspection is mainly focused on technical issues including data transmission, video and image analysis, etc. (Zhang, Yuan, Li et al., 2017; Zhang, Yuan, Fang et al., 2017; Jiang et al., 2017), while routing algorithm analysis is mostly ignored. Most existing routing algorithms are dedicated to pathfinding for a single object that needs to travel from a given start point to an end point. However, they cannot be directly used to guide multiple objects (i.e., the ground support team and the UAV in this thesis). The motions and locations of these objects need to be carefully coordinated under various constraints. Specifically, two coordination issues in this problem need to be addressed. They are 1) the trade-off between over-deployment of the ground team and non-data transmission of UAV, and 2) the trade-off between the number of ground stations and the capacity of the power system. By addressing these two issues, the proposed algorithm can be applied to handle a more complex routing problem with multiple objects. It can offer a paradigm to coordinate the motion of two different parties (e.g., the UAV and the ground team) under the required constraints.

There exists an algorithm for transmission line inspection using a suspended robot that considers the motion coordination between the suspended robot and the ground team

(Nagarajan et al., 2017). There are some similarities between the suspended-based robot and the UAV in transmission line inspection. For instance, a range limitation of live data transmission requires the ground team to dynamically change their location to keep themselves within the required range (Montambault and Pouliot, 2012) and ensure that live signals can be received and processed, robot motion can be controlled, and the health condition of the line can be captured. However the ground team must navigate the UAV back to the ground station for battery replacement, while the suspended robot could stay on the power line and wait for the battery replacement.

In this thesis, we focus on the routing algorithm for inspecting transmission systems using UAVs to enhance the cost-effectiveness in critical infrastructure maintenance. A cost model for the transmission line inspection with UAVs is proposed. Both lithium batteries and hydrogen fuel cell are considered for the power system of the UAVs in this analysis. The remaining part of this thesis is organized as follows. In Section 2, related works are briefly reviewed. In Sections 3 and 4, a heuristic routing algorithm and an analytical routing algorithm are proposed, respectively. Finally, conclusions are drawn, and future work is discussed in Section 5.

2. LITERATURE REVIEW

In this section, we briefly review literature in the relevant areas including UAV technology, routing algorithm, robot path planning, and Particle Swarm Optimization (PSO).

2.1. UAV TECHNOLOGY APPLICATION

UAVs, which are aircraft without a human pilot aboard, have been widely adopted in many fields such as pollution monitoring, filmmaking, and reconnaissance. For example, Alvear et al. (2017) proposed a solution to allow UAVs to autonomously trace pollutant sources and monitor air quality in the surrounding area. However, they found that the proposed solution was excessively time-consuming. Therefore, they improved the solution by adopting a space discretization technique (Alvear et al., 2018).

UAVs have also been used as a possible approach for transmission line inspection. Wang et al. (2009) presented an applied inspection robotic system based on an unmanned autonomous helicopter for power line corridor inspection. Later, they presented an applied inspection robot called SmartCopter, which was based on an unmanned autonomous helicopter, for the inspection of transmission lines (Wang et al., 2010). Yang et al. (2012) studied overhead power line detection from UAV video images. Li et al. (2016) proposed a transmission line intelligent inspection central control and mass data processing system and application based on UAV.

The prevalent electric power storage technology used by UAVs is the lithium battery. Many other power systems or recharging methods for supporting UAVs have

been studied in recent years. They include a solar power system (Shiau et al., 2009) and wireless charging (Xu et al., 2018). However, most of them are not commercialized. One of the novel power systems that has been commercialized is the fuel cell power system used by UAV. The typical fuel energy system is a hydrogen fuel cell system, which was studied by Veziroğlu and Şahin in 2008. The usage for UAV has been designed and investigated by Gadalla and Zafar in 2012, and Kim and Kwon in 2012.

2.2. ROUTING ALGORITHMS

In engineering studies, the routing algorithm determines the best route from a start point to an end point. Many studies in this area have been reported. For example, the routing problem of a bridge inspection team departing from the depot, visiting bridges, finding lodging accommodations, and returning to the depot was optimized by ant colony optimization (Huang et. al., 2018). The freeway service patrol problem involving patrol routing design and fleet allocation on freeways was investigated using a genetic algorithm incorporated with a niche strategy (Sun et al., 2018). The routing issue of large size traveling salesman problems with 500-100,000 cities was studied using an algorithm based on the concept of Tabu search (Fiechter, 1994). A heuristic algorithm named Harmony Search, which mimicked the improvisation of music players was used to investigate the routing planning in a traveling salesman problem (Geem et al., 2001). A branch-and-bound algorithm for the double traveling salesman problem was studied by Carrabs et al. in 2013. A systematic comparison in terms of computational cost between various heuristic algorithm and the traditional algorithm was also conducted (Sharma et al., 2012).

2.3. ROBOT PATH PLANNING

In the area of robot path planning, various routing algorithms using classic approaches such as cell decomposition, potential field, sampling-based method, and sub-goal network have been proposed. For example, the applications of robot path planning based on cell decomposition can be found in the literature (Rosell, 2005; Šeda, 2007). A potential field method, inspired by the concept of electrical charges, was used to guide the robot to move toward the target while pushing away from the obstacles by assigning repulsive and attractive forces to the obstacles and the goal, respectively (Cosio and Castaneda, 2004). Sampling-based motion planning (SBP) algorithms create the paths by randomly adding points instead of evaluating all possible solutions. Two possible SBPs, probabilistic road-map and rapidly exploring random trees have been investigated (Lee et al., 2014). The sub-goal network utilizes a list of reachable configurations from the starting point to a goal point while avoiding all obstacles to identify the path for robot motion. This method has been used in a motion planner for humanoid robots (Candido et al., 2008) and for deploying the vision system and IR sensors (Singh et al., 2011; Liu et al., 2010).

In addition to these classic approaches, heuristic-based algorithms such as neural networks, fuzzy logic, and nature-inspired methods have recently been proposed. A neural network was used to determine the free space and a safe direction for the next robot section of the path in the workspace (Janglova, 2004). A four-layer neural network dealing with the tasks of learning, adaptation, generalization, and optimization has been used to solve the path and time optimization for the robot (Parh and Singh, 2009). A fuzzy logic controller is used to control the robot's motion along the predefined path (Peri

and Simon, 2005). Motion control for autonomous robot navigation using fuzzy logic and the stereo vision-based path-planning module was investigated (Foudil et al., 2014). Nature-inspired methods such as genetic algorithms, particle swarm optimization, and ant colony optimization have also been successfully applied in robot path planning (Mac et al., 2016).

2.4. PARTICLE SWARM OPTIMIZATION

Particle swarm optimization (PSO) is a nature-inspired method initially proposed by Kennedy and Eberhart (1995). The particles in a given swarm are used to form a population of candidate solutions. The location of each particle is updated iteratively according to its distance to the particle with the best location in the entire swarm as well as the best location that has been visited by itself. The quality of the location is evaluated by a fitness function. The algorithm stops when the given iteration number is achieved and a near optimal solution can be identified.

PSO has been widely used to solve high dimensional optimization problems to obtain a near optimal solution in many areas such as financial forecasting, motion tracking, path planning, scheduling in manufacturing, etc.

For forecasting in finance, a great deal of research has been reported. For example, a predicting model for forecasting stock market behavior with the aid of locality preserving projection, particle swarm optimization, and a support vector machine was constructed by Guo et al. in 2013. A method to forecast market trends to emulate the way real traders make predictions based on an adaptive network-based fuzzy inference system was proposed by Bagheri et al. in 2014. Quantum-behaved PSO was used in Bagheri's

model for tuning the adaptive network-based fuzzy inference system membership functions. Accurate forecasting of volatility from a financial time series was studied based on a PSO trained quantile regression neural network in (Pradeepkumar and Ravi, 2017).

For motion tracking, the studies are briefly reviewed as follows. A simplified-belief hybrid PSO method propagating the weights of limb observations to the corresponding particles along the edges of the body model is proposed for tracking marker-less human poses in monocular videos of human motion in (Jun, 2014). A method for high-dimensional search space involved in the marker-less full-body articulated human motion tracking problem based on hierarchical multi-swarm cooperative particle swarm optimization was developed in (Saini et al., 2015) to overcome the limitation of premature convergence.

In the area of path planning for the robot, Han et al. (2016) used PSO to identify the path for multi-robot systems to reach the targets without collision not only between the robots but also between the robots and the environment. Robot path planning for rescuing multiple survivors in a limited time frame was proposed and solved using PSO in (Geng et al., 2014).

The PSO has also been used to identify the optimal scheduling for a manufacturing system. For example, PSO was used to solve a mathematical model for identifying an optimal participation strategy in a demand response program designed for mitigating electricity over-generation due to the high usage of renewable sources in electricity grid in (Islam et al., 2018). A combined production scheduling model that simultaneously considers energy control and maintenance implementation to address the

concerns of energy consumption, intelligent maintenance, and throughput improvement was proposed and solved using PSO in (Sun et al., 2018). An integrated electricity demand response model for combined manufacturing, heating, venting, and air-conditioning systems is proposed and solved in (Sun et al., 2016).

Apart from the aforementioned areas, PSO has been involved in many other unique problems. For example, another application of PSO is to find the optimal location of flexible AC transmission system devices with a minimum cost of installation to improve system load ability, which was presented in (Saravanan et al., 2007). An optimal power management approach for plug-in hybrid electric vehicles in uncertain driving conditions was proposed and solved by PSO to optimize the threshold parameters of the rule-based power management strategy under a certain driving cycle (Chen et al., 2016). Onwunalu and Durlinsky (2010) used a PSO algorithm for determining the optimum type and location of new wells, which is an essential component in the efficient development of oil and gas fields.

3. HEURISTIC MODEL

In this section, we first propose a heuristic routing algorithm for using UAVs in transmission line inspection. Then, cost models are presented for the lithium battery power system and hydrogen fuel cell power system. A numerical case is used to illustrate the performance with respect to the cost-effectiveness for these two power systems using the proposed routing algorithm. In addition, the comparison of total cost between the suspended robot and the UAV is shown at the end of the section.

3.1. HEURISTIC ROUTING ALGORITHM

The general routing algorithm for guiding the ground support team in the inspection is shown in Figure 3-1. The ground team needs to prepare the apparatus of the inspection when the ground team reaches the ground station. The UAV will first take off at the station and fly back r distance to the start point of the inspection of this round with the maximum flying velocity v_2 (step 1 in Figure 3-1). Then, UAV starts to inspect $2r$ distance over the inspection line with the inspection velocity v_1 (step 2 in Figure 3-1). Note that since UAV needs to take photos in inspection, v_1 is less than v_2 . Here, we define r as the feasible flight radius, which is determined by the capacity of the power system or the communication and control distance of the UAV. Let $r_{control}$ be the maximum feasible flight radius within the communication and control distance of UAV; $r_{capacity}$ be the maximum feasible flight radius that one battery can cover. r can be formulated as:

$$r = \min(r_{control}, r_{capacity}) \quad (1)$$

Let d_{max} be the maximum feasible inspection distance that one battery or fuel tank can support, i.e., $d_{max}=2r$. After the $2r$ distance is covered, the UAV flies back and lands at the ground station with a velocity of v_2 (step 3 in Figure 3-1). Such a procedure is defined as an inspection round in this thesis. It is reasonable to assume that v_1 is the same, while v_2 is different for the UAVs with different power systems. Let v_2^b and v_2^c be the maximum flying velocities of the UAVs using lithium battery and hydrogen fuel cell, respectively. Finally, the ground team needs to pack the apparatus and replace the battery or fuel tank if needed (step 4 in Figure 3-1) and relocate the ground team to the next station with the average motion velocity of the vehicle v_3 (step 5 in Figure 3-1).

3.1.1. For the UAV Powered by the Lithium Battery. Generally, the UAV powered by the lithium battery cannot support the flying distance as far as its communication and control distance. Thus, the UAV powered by the lithium battery needs to land for replacing the battery. The feasible flight radius for the UAV powered by lithium battery r_c is its maximum feasible flight radius that one battery can cover, i.e., $r_{capacity}^b$. The lithium battery is replaced by the ground team at each ground station as shown in step 4 of Figure 3-1. After the replacement, the replaced battery starts to be recharged by the charging equipment inside the ground vehicle and the ground vehicle moves forward to the next station for the relocation. Thus, the maximum feasible inspection distance d_{max}^b of the UAV when the lithium battery is used is $2r_{capacity}^b$.

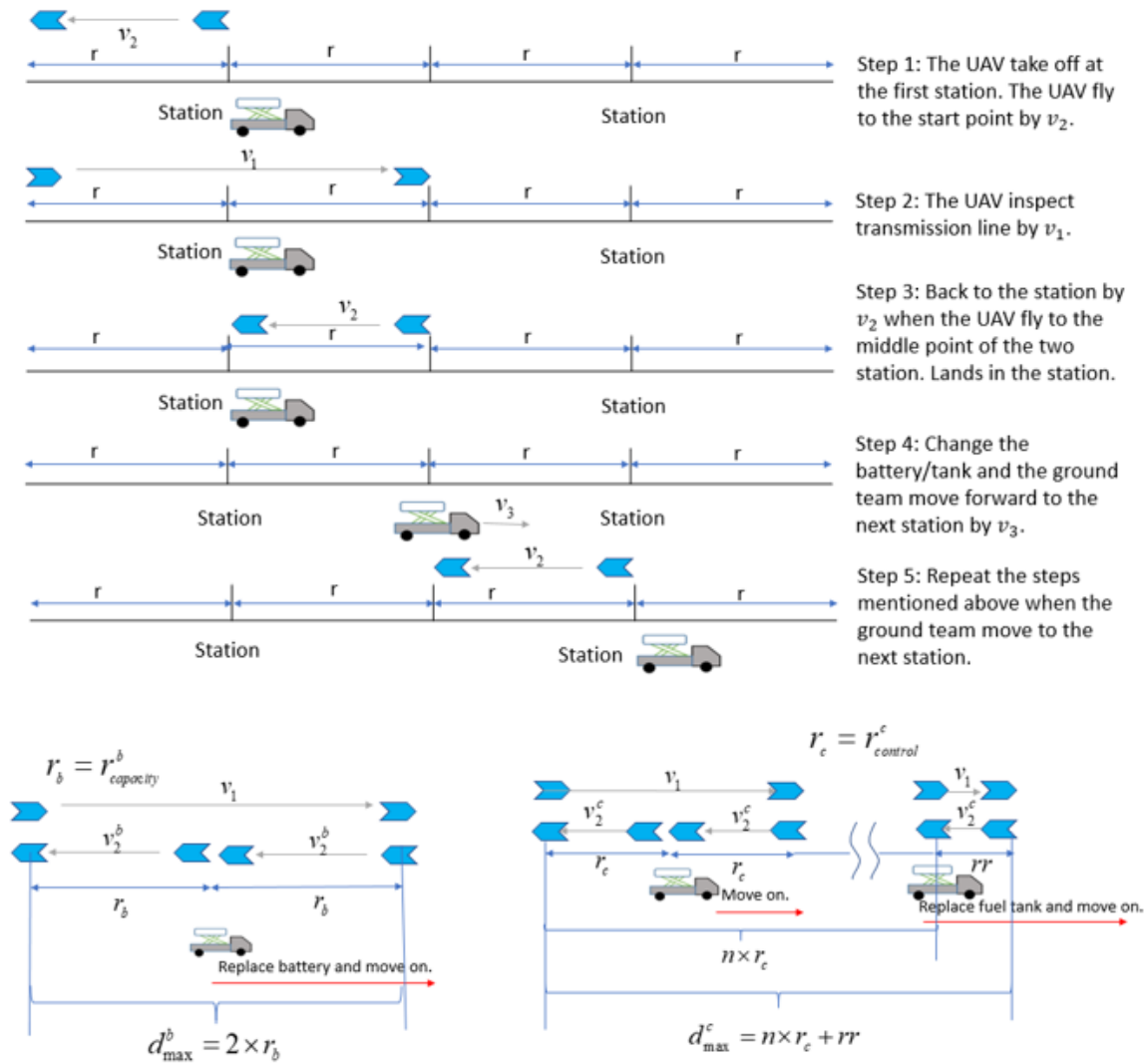


Figure 3-1. The General Method of the Inspection

Typically, the parameter of $r_{capacity}^b$ is not given directly by the UAV manufacturers, instead, the maximum flight time $t_{flighttime}^b$ that a lithium battery can support is usually given as a critical parameter to demonstrate the power endurance, which can be presented as:

$$\frac{r_{capacity}^b}{v_2^b} + \frac{2r_{capacity}^b}{v_1} + \frac{r_{capacity}^b}{v_2^b} = t_{flighttime}^b \quad (2)$$

Therefore, r_b can be calculated by:

$$r_b = r_{capacity}^b = \frac{t_{flighttime}^b \times v_1 \times v_2^b}{2 \times (v_1 + v_2^b)} \quad (3)$$

3.1.2. For the UAV Powered by Hydrogen Fuel Cell. Generally, for the UAV powered by a hydrogen fuel cell, the capacity of the fuel cell can support a much longer flying distance than the lithium battery does. The feasible flight radius based on the capacity of one fuel tank is typically longer than its communication and control distance. Therefore, the feasible flight radius for the UAV powered by a hydrogen fuel cell r_c is

$$r_{control}^c.$$

Since that, after completing one round inspection, the remaining capacity of the fuel tank can support the UAV to inspect additional transmission lines. The ground team doesn't need to replace the fuel tank at the ground station if the remaining capacity of the fuel tank can support the next round or the remaining distance of the trip. Let d_{max}^c be the maximum feasible inspection distance that one fuel tank can support. We can assume that d_{max}^c is between n and $n+1$ times of r_c (typically, $n \geq 2$). Let rr be the remaining distance that can be covered by the remaining capacity of the fuel cell after the UAV covers the distance of nr_c . Thus, n and d_{max}^c can be calculated by:

$$d_{max}^c = n \times r_c + rr \quad (4)$$

Let $t_{flighttime}^c$ be the maximum flight time of an inspection round for the UAV

powered by the fuel cell, which can be calculated by:

$$n \times \left(\frac{r_c}{v_1} + \frac{r_c}{v_2^c} \right) + \frac{rr}{v_1} + \frac{rr}{v_2^c} = t_{flighttime}^c \quad (5)$$

$t_{flighttime}^c$ can thus be formulated by:

$$\frac{n \times r_c + rr}{v_1} + \frac{n \times r_c + rr}{v_2^c} = t_{flighttime}^c \quad (6)$$

Substitute the numerators on the left-hand sides of (6) using (4), d_{max}^c can be obtained by:

$$d_{max}^c = \frac{t_{flighttime}^c \times v_1 \times v_2^c}{v_1 + v_2^c} \quad (7)$$

The above discussion is based on the scenario that the total inspection distance D is larger than the distance of one inspection round. $\frac{D}{2}$ can be used as the flight radius if D is less than $2r_c$ or $2r_b$.

3.2. COST MODEL

The formulations of each cost component for both lithium battery and hydrogen fuel cell powered UAVs are shown in Table 3-1.

In Table 3-1, S_{dr} and S_{te} are the salary rates for the driver and the technician in the ground team. T_{Total}^b and T_{Total}^c are the total times for the inspection using UAV with lithium battery and hydrogen fuel cell, respectively. T_u^b and T_u^c , are the working times of the UAV powered by lithium battery and hydrogen fuel cell, respectively. T_g is the total

Table 3-1. Cost Component and Formulation

	Cost component/notation		Lithium Battery	Hydrogen Fuel Cell
1	Salary	C_{st}	$C_{st}^b = (S_{dr} + 2S_{le}) \times T_{Total}^b$ $= (S_{dr} + 2S_{le}) \times (T_u^b + T_g^b + T_s^b + T_c)$	$C_{st}^c = (S_{dr} + 2S_{le}) \times T_{Total}^c$ $= (S_{dr} + 2S_{le}) \times (T_u^c + T_g^c + T_s^c + T_c)$
2	Setup	C_s	$C_s^b = C_{si} + C_{sb} + C_{sg}^b$ $= C_{si} + c_{sb} \times N_r^b + c_{sg} \times N_g^b$	$C_s^c = C_{si} + C_{sc} + C_{sg}^c$ $= C_{si} + c_{sc} \times N_r^c + c_{sg} \times N_g^c$
3	Battery/Cell	C_{bd} / C_{cd}	$C_{bd} = G_s \times \frac{T_u^b}{L_s} + \sum_{m=1}^M G_b \times \frac{t_b^m}{L_b}$	$C_{cd} = G_h \times Q + \sum_{q=1}^Q G_t \times \frac{t_l^q}{L_t} + G_c \times \frac{T_u^c}{L_c}$
4	Data Transmission	C_{dd}	$C_{dd} = G_d \times \frac{T_u^b + T_s^b}{L_d}$	$C_{dd} = G_d \times \frac{T_u^c + T_s^c}{L_d}$
5	Auxiliary Equipment	C_{ae}	$C_{ae} = G_a \times \frac{T_u^b + T_s^b}{L_a}$	$C_{ae} = G_a \times \frac{T_u^c + T_s^c}{L_a}$
6	UAV	C_{ud}	$C_{ud} = G_u \times \frac{T_u^b}{L_u}$	$C_{ud} = G_u \times \frac{T_u^c}{L_u}$
7	Ground Travel	C_{gt}	$C_{gt} = c_{gt} \times D$	

travel time of the ground team. T_s^b and T_s^c are the total setup time of the ground team for relocation when using lithium battery and hydrogen fuel cell, respectively. T_c is the final close time of the ground team. C_{si} is the cost of the initial setup to start the inspection task. C_{sb} and C_{sc} are the total setup costs of battery replacement and fuel tank replacement, respectively. C_{sg}^b and C_{sg}^c are the total setup costs of the ground team relocation when using UAV with lithium battery and hydrogen fuel cell, respectively. c_{sb} and c_{sc} are the cost required for one setup of battery and fuel tank replacement, respectively. N_r^b and N_r^c are the times of replacement of the lithium battery and hydrogen fuel tank, respectively. c_{sg} is the cost required for one setup of the ground team relocation. N_g^b and N_g^c are the relocation times of the ground station for UAV powered by lithium battery and hydrogen fuel cell, respectively. G_s is the cost of charging equipment

and L_s is the expected lifetime of charging equipment. G_b is the cost of one lithium battery. L_b is the expected lifetime of one lithium battery. M is the number of lithium batteries that the inspection trip needs. t_b^m is the total operating time for the m^{th} lithium battery during the trip. G_h is the cost of the refueling for each hydrogen fuel tank. Q is the number of fuel tanks that the inspection trip needs. G_t and G_c are the costs of hydrogen tank and hydrogen fuel cell, respectively. t_t^q is the total operating time of the q^{th} fuel tank. L_t and L_c are the expected lifetimes of tank and cell, respectively. G_d is the cost of the data transmission system. L_d is the expected lifetime of the data transmission system. G_a is the cost of the auxiliary equipment. L_a is the expected lifetime of the auxiliary equipment. D is the inspection distance. c_{gt} is the ground travel cost per unit distance. G_u is the cost of the UAV. L_u is the expected lifetime of the UAV.

The rest of this section illustrates the details of the different elements in Table 3-1 including the total travel time of the ground team T_g , the working time T_u^b and T_u^c , the total setup time T_s^b and T_s^c , and the battery depreciation cost C_{bd} and the cell depreciation cost C_{cd} .

3.2.1. Total Travel Time of the Ground Team. It can be formulated as:

$$T_g = \frac{D}{v_3} \quad (8)$$

3.2.2. Working Time. Based on equation (2)-(7), the working time T_u^b and T_u^c can be inferred by

$$T_u^b = \frac{D}{v_1} + \frac{D}{v_2^b} \quad (9)$$

$$T_u^c = \frac{D}{v_1} + \frac{D}{v_2^c} \quad (10)$$

3.2.3. Total Setup Time. For the lithium battery, the total setup time can be formulated as:

$$T_s^b = T_{sr}^b + T_{sg}^b \quad (11)$$

where T_{sr}^b is the total lithium battery replacement time, T_{sg}^b is the total preparation and packing time of ground team relocation. The total battery replacement time can be calculated by the unit time per battery replacement t_{sr}^b and the times of battery replacement N_r^b . The preparation and packing time depends on unit time per preparation and packing t_{sg}^b and the times of the ground team station relocation N_g^b , i.e.,

$$T_s^b = t_{sr}^b \times N_r^b + t_{sg}^b \times N_g^b \quad (12)$$

The times of the lithium battery replacement N_r^b and the relocation times of the ground stations N_g^b can be calculated by the inspection distance D and the feasible radius of flight r_b as follows:

$$N_r^b = N_g^b = \left\lceil \frac{D}{2r_b} \right\rceil \quad (13)$$

where $\lceil \cdot \rceil$ is ceiling function.

For the hydrogen fuel cell, similarly, the total setup time can be formulated as:

$$T_s^c = T_{sr}^c + T_{sg}^c \quad (14)$$

where T_{sr}^c is the total hydrogen fuel tank replacement time, T_{sg}^c is the total preparation and packing time of ground team relocation for UAV with a hydrogen fuel cell. The

preparation and packing time depends on unit time per preparation and packing t_{sg}^c and the number of the ground team station N_g^c . The total hydrogen fuel tank replacement time can be calculated by the unit time per hydrogen fuel cell replacement t_{sr}^c and the number of tank replacement N_r^c . Therefore, the total setup time can be formulated as:

$$T_s^c = t_{sr}^c \times N_r^c + t_{sg}^c \times N_g^c \quad (15)$$

From Figure 3-1, because $2r_c$ is the distance of one inspection round, N_g^c can be formulated as:

$$N_g^c = \left\lceil \frac{D}{2r_c} \right\rceil \quad (16)$$

In this thesis, we stipulate that the UAV replaces the fuel tank after $n \times r_c$ inspection distance and uses a new tank for next $n \times r_c$ inspection distance. As shown in Figure 3-2, the D_{left} is the remaining distance after $k \times n \times r_c$ inspection distance is covered. If D_{left} is larger than rr , the $(k+1)^{th}$ fuel tank is used to continue the remaining trip. While the k^{th} fuel tank is used to finish this trip if D_{left} is not larger than rr . Thus, N_r^c can be calculated as:

$$N_r^c = \begin{cases} k, & \text{if } D_{left} \leq rr \\ k+1, & \text{else} \end{cases} \quad (17)$$

$$k = \left\lfloor \frac{D}{n \times r_c} \right\rfloor \quad (18)$$

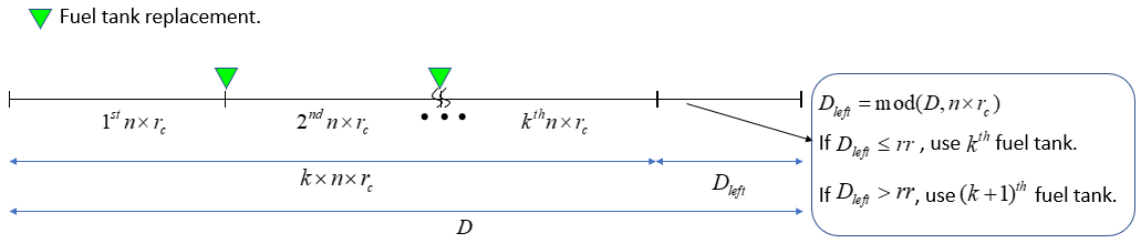


Figure 3-2. Fuel Tank Replacement

3.2.4. Battery Depreciation Cost. In Table 3-1, the total operating time of each lithium battery t_b^m is required for calculating the battery depreciation cost. The lithium battery can be recharged using the charging equipment during the inspection. The recharging time $t_{recharge}$ varies regarding the capacity of the battery and the electric current. The lithium battery power system is illustrated in Figure 3-3.

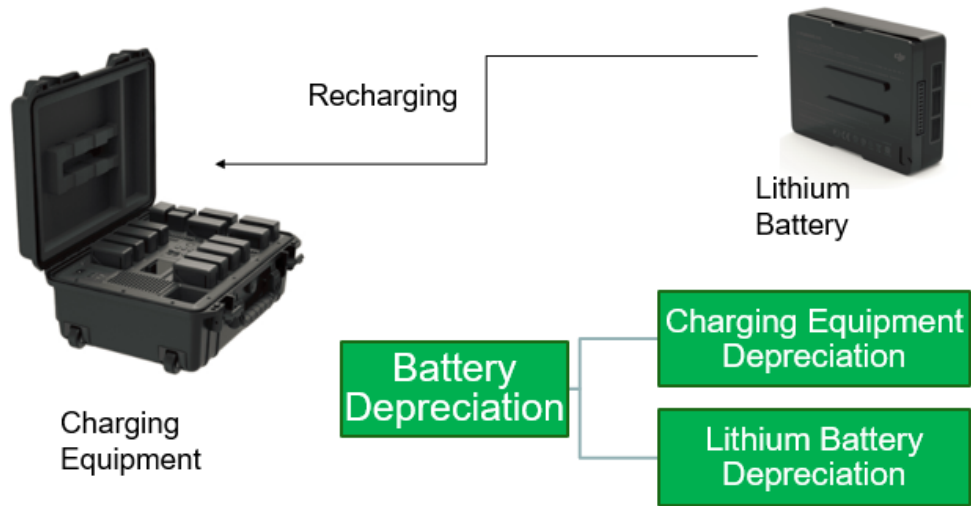


Figure 3-3. Lithium Battery Power System and Cost Components

The overall inspection trip can consist of several inspection rounds. For each inspection round, the UAV is operated to finish the inspection round with a fully

recharged battery, which will be replaced and recharged after this inspection round. After packing, the UAV is moved forward to the next station and the same task using the other fully recharged battery is conducted. For the specific inspection trip, it consists of $i \times M$ rounds along with residual distance L as shown in Figure 3-4 where i is the number of cycles where all batteries are used and recharged. M is the number of batteries necessary for covering the whole inspection.

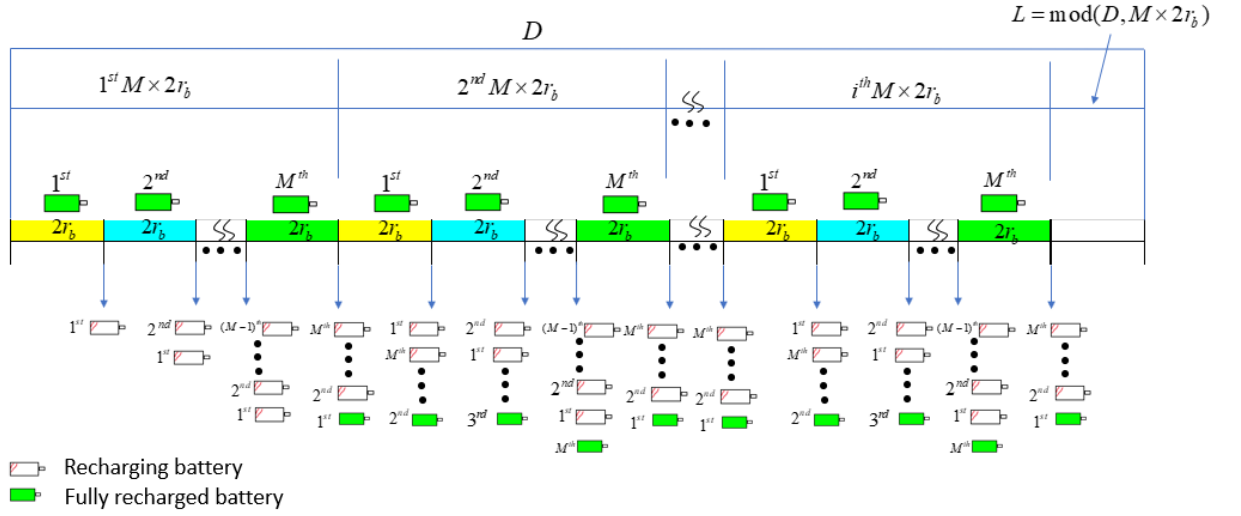


Figure 3-4. Lithium Battery Recharging Illustration

M can be calculated based on the recharging time $t_{recharge}$ and the total flight time

t_{flight}^M of the M batteries. The total flight time t_{flight}^M is the sum of the working time of the

UAV, the travel time of the ground team, the total replacement time and the preparation and packing time of ground team relocation of these M batteries. Based on (8), (9) and

(12), t_{flight}^M can be formulated as:

$$t_{flight}^M = \frac{2r_b \times M}{v_3} + \left(\frac{2r_b \times M}{v_1} + \frac{2r_b \times M}{v_2^b} \right) + (t_{sr}^b \times M + t_{sg}^b \times M) \quad (19)$$

Since $t_{recharge}$ is within range of $(t_{flight}^{M-1}, t_{flight}^M]$, M can be formulated as:

$$M = \left\lceil \frac{t_{recharge}}{\frac{2r_b}{v_3} + \left(\frac{2r_b}{v_1} + \frac{2r_b}{v_2^b} \right) + (t_{sr}^b + t_{sg}^b)} \right\rceil \quad (20)$$

After the UAV completes its inspection round with the M^{th} battery, the 1st battery can be fully recharged. This is called as a cycle based on battery usage. It can be calculated by:

$$i = \left\lfloor \frac{D}{M \times 2r_b} \right\rfloor \quad (21)$$

For the m^{th} battery, the operation time it_b^m of the $i \times M \times 2r_b$ inspection distance can be calculated by:

$$it_b^m = i \times t_{flighttime}^b \quad (22)$$

For the m^{th} battery, the operation time Lt_b^m of the operation time of the L distance can be calculated by:

$$Lt_b^m = \max(\min(L - (m-1) \times 2r_b, 2r_b), 0) \times \left(\frac{1}{v_1} + \frac{1}{v_2^b} \right) \quad (23)$$

The total operation time t_b^m for m^{th} battery can be calculated by the sum of the operation time of the $i \times M \times 2r_b$ inspection distance it_b^m and the operation time of the L distance Lt_b^m :

$$t_b^m = it_b^m + Lt_b^m \quad (24)$$

3.2.5. Cell Depreciation Cost. As shown in Table 3-1, the hydrogen fuel cell depreciation cost can be calculated using the cost of refueling each hydrogen fuel tank G_h , the cost of each hydrogen tank G_t , the number of fuel tank that the inspection trip needs Q , the total operating time t_i^q for the q^{th} tank, the expected lifetime of each tank L_t , the cost of one hydrogen fuel cell G_c , the working time of UAV T_u^c , and the expected lifetime of the hydrogen fuel cell L_c . The hydrogen fuel cell power is illustrated in Figure 3-5.

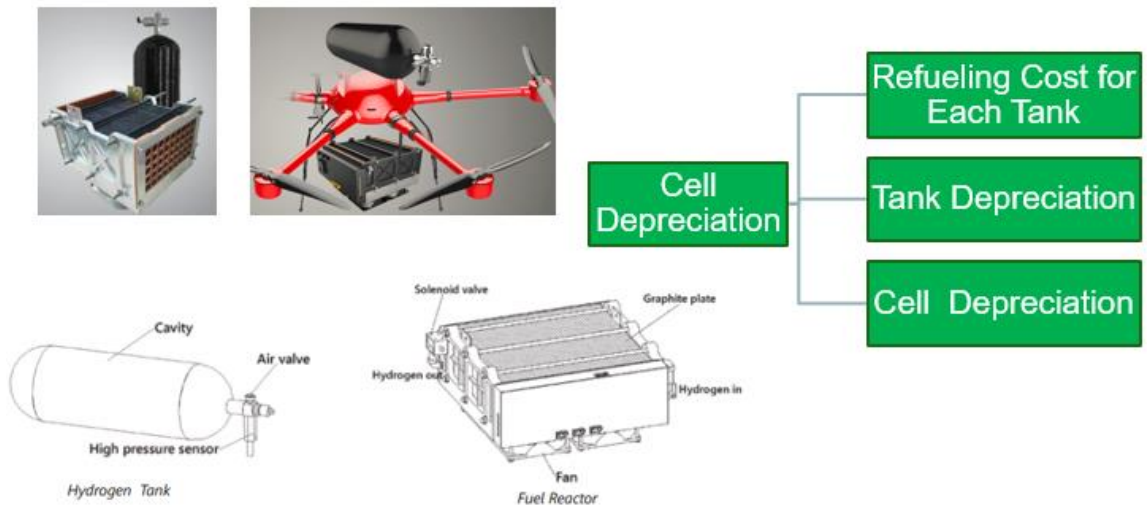


Figure 3-5. Hydrogen Fuel Cell Power System and Cost Components

Here, the cost of the hydrogen fuel cell denotes the cost of the whole hydrogen fuel cell system except hydrogen tank, including the fuel reactor, control system, lithium battery, etc. The expected lifetime of one cell is L_c .

For the hydrogen fuel cell, it's unrealistic to refuel the cells during the trip, even though it's an extreme short time for refueling comparing with the recharging time of

lithium battery (Yang, 2009). The current U.S. Department of Energy (DOE) technical target of refueling time for 2020 of an onboard hydrogen tank is 3 min for 5 kg of hydrogen (DOE, 2017). In the next content of this section, this thesis will discuss how to calculate the total operating time t_i^q for the q^{th} tank.

Based on Figure 3-4, the number of tanks prepared, Q , is equal to the number of cells replacement N_r^c . When D_{left} is less than or equal to rr , the last tank can support the last nr_c plus the remaining rr distance, while the other tanks are used to support the earlier nr_c distances. When D_{left} is large than rr , the last tank supports D_{left} distance, the other tanks support the earlier nr_c distances. Therefore, the total operating time t_i^q for the q^{th} tank can be calculated as follows:

$$t_i^q = \begin{cases} \left(\frac{nr_c}{v_1} + \frac{nr_c}{v_2^c} \right) + \left\lfloor \frac{q}{Q} \right\rfloor \times \left(\frac{D_{left}}{v_1} + \frac{D_{left}}{v_2^c} \right), & \text{if } D_{left} \leq rr \\ \left(\left\lfloor \frac{q}{Q} \right\rfloor - 1 \right) \times \left(\frac{nr_c}{v_1} + \frac{nr_c}{v_2^c} \right) + \left\lfloor \frac{q}{Q} \right\rfloor \times \left(\frac{D_{left}}{v_1} + \frac{D_{left}}{v_2^c} \right), & \text{else} \end{cases} \quad (25)$$

3.3. CASE STUDY

In this section, we calculate and analyze the total costs of using UAVs powered by a lithium battery and hydrogen fuel cell for inspecting the transmission lines with four different distances (10 km, 30 km, 38 km, 45 km) using the proposed cost model. The assumptions for the parameters used in this case study are as follows.

- The inspection velocity v_l and the moving velocity v_3

Refer to (Wang et al. 2010), the UAV's flying speed can be 15 km/h (i.e., 4.17 m/s), so

here the average velocity of the UAV during inspection v_l was assumed as 4 m/s. The average moving velocity of the ground team vehicle v_3 was assumed as 13m/s.

- The maximum flight time $t_{flighttime}^b$

For the UAV powered by lithium battery, based on some UAVs in the market (DJI MATRICE 210, Aeryon SkyRanger, ING Responder and Microdrones MD MAPPER 1000), the maximum flight time is between 38 min and 50 min with no payload. Based on (DJI website, 2017), the flight time $t_{flighttime}^b$ was assumed to be 25 min.

- The average flying velocity v_2^b

The maximum speed of some UAVs powered by lithium battery is around 17m/s, considering the wind and uncertainties, the average velocity v_2^b was assumed as 15m/s.

- The feasible flight radius r_b

For the most existing UAVs in the market, the control distance varies from 5 km to 10 km. However, the capability of a lithium battery of the UAV cannot cover such a long distance. Using assumptions about the velocity and the flight time r_b could be obtained with the value of 2.3 km.

- The maximum flight time $t_{flighttime}^c$

For the UAV powered by a hydrogen fuel cell, the flight time depends on the capacity of the fuel cell, the wind, the payload, etc. There are not too many hydrogen powered UAVs

in the market, so referring to the MMC HyDrone 1550 UAV and H1-Fuel Cell (MMC website, 2017). The endurance is about 150 min with a nine-liter tank. Considering the effective availability in the actual operation, here, the maximum flight time $t_{flighttime}^c$ for one hydrogen fuel cell was assumed as 120 min.

- The average flying velocity v_2^c

In the experiment of (Gadalla & Zafar. 2012) and (Kim & Kwon. 2012), the speeds of the cruise phase were 17 m/s and 8.33-13.89 m/s, respectively. The maximum speed of MMC HyDrone 1550 is 10m/s. It is a safe assumption to choose the average velocity v_2^c to be 8 m/s.

- The feasible flight radius r_c

The maximum control distance of MMC HyDrone 1550 is 10 km which is much shorter than the feasible flight radius that the capacity of one fuel tank can support, so let r_c be 8 km be a safe assumption.

- Others

Assume the unit time per battery or tank replacement t_{sr}^b and t_{sr}^c both to be 10 min.

Assume unit time per preparation and packing t_{sg}^b and t_{sg}^c both to be 20 min. Assume the cost required for each setup of the ground station and battery or cell replacement c_{sg} , c_{sb} and c_{sc} all to be \$17. They are assumed based on the estimation from our industrial collaborator according to some other similar existing tasks that have been widely

conducted. For example, the station setup time was estimated based on the setup time of the ground team when using a robotic arm for maintaining the transmission line. The battery change time was estimated based on the recorded data of other equipment where battery change is required.

- The salary rates are estimated by referring to the existing pay rates of similar positions in the U.S. as well as the feedback from an industrial collaborator. For example, the average hourly wage for a truck driver - heavy in the United States is \$21 (Truck Driver - Heavy in the United States). Thus, we assumed the hourly salary rate of the driver is \$25/h. The range of the average hourly pay for a Hardware Engineer III in the United States is between \$43 and \$53 (Hardware Engineer III in the United States). Thus, we assumed the technician staff salary cost is \$45/hour.

The results of total time for the inspection and the salary cost are presented in Table 3-2. Comparing the total time for the inspection to the results from (Nagarajan et al., 2017) where suspended robot is used in transmission line inspection, when UAV is used instead of suspended robot, operation time can be significantly saved due to the faster velocity and the avoidable time for crossing the possible obstacles. Considering an 8-hour working day, only about 10 km could be inspected for if the suspended robot is used, but more than 30 km could be done in one day if UAV is used.

Table 3-2. The Result of Total Time for the Inspection and the Salary Cost

	Lithium battery				Fuel cell			
	10km	30km	38km	45km	10km	30km	38km	45km
T_u (hours)	0.88	2.64	3.34	3.96	1.04	3.13	3.96	4.69
T_g (hours)	0.21	0.64	0.81	0.96	0.21	0.64	0.81	0.96
T_s (hours)	1.50	3.50	4.00	5.00	0.50	1.00	1.50	1.50
T_c (hours)	1.00	1.00	1.00	1.00	1.00	1.00	1.00	1.00
Total time (hours)	3.59	7.78	9.15	10.92	2.76	5.77	7.27	8.15
Salary Cost (\$)	377.30	816.89	961.23	1,146.58	289.32	605.43	763.38	855.65

Assume the recharging time of the lithium battery is 90 min, then, in this case, M is 2. The purchase costs and expected lifetime/working times of the UAV, data transmission system, lithium battery, fuel cell, and auxiliary equipment are listed in Table 3-3.

Table 3-3. Parameters for Equipment Involved in Operation

	Purchase cost (\$)	Expected lifetime/working time (hours)
UAV	20,000	5,000
Lithium Battery	1,000	1,000
Charging Equipment	1,500	5,000
Fuel Cell	1,000	5,000
Fuel Tank	300	5,000
Tank Refueling	10	-
Data Transmission System	1,200	4,000
Auxiliary Equipment	4,200	5,000

Using UAV for the transmission line inspection is still an emerging area, thus, some critical technical parameters for the equipment itself is not allowed to be exposed without the permission from the manufacturers due to the concerns of commercial confidentiality. The empirical data relevant to the use of the equipment in real operation are not completed since there is still not a wide adoption yet. In this thesis, such data are estimated referring to some publicly available data belong to some similar equipment or similar operations. The costs are estimated using the data available to the similar equipment used in similar areas. The lifetimes are estimated using the warranty period offered by similar products. It is suggested by our industrial collaborator that it is appropriate to be conservative for an emerging technology. All these assumptions have been verified by our industrial collaborator with an internal project report. The details of the estimations in Table 3-3 are provided as follows.

In Table 3-3, the UAV purchase cost is estimated as follows. The right drone at the right price point depends entirely on the area of expertise. Even within the same area applications, there is significant variation depending upon where it is operated. The price ranges from \$1,500 to well over \$25,000. Here, we assumed the purchase cost of a UAV is \$20,000. We prefer to estimate the lifetime based on the warranty period of a similar product to obtain a conservative estimation. Referring to the warranty period (12 months) of a product (After-sales service policies, 2018), we assume the lifetime to be 5,000 hours. It is around twice the usage of the warranty period if we assume 10 hours per working day, 22 working days per month.

The battery cost is estimated based on the information of the same type of lithium-ion battery. One kind of lithium-ion battery used for UAV cost \$370 (Matrice 200

series, 2017; TB55, 2018) and one of the UAV products needs to be supported by two lithium batteries (Matrice 200 series, 2017). Thus, the battery cost is estimated to be around \$1,000, considering some other fees such as tax.

The lifetime of the battery is estimated similarly based on the warranty period of the battery used by UAV for the utility system. The typical warranty period reported is 200 charging cycles (After-sales service policies, 2018). The literature also shows that lithium-ion batteries typically have the lifespan of between 300 and 500 cycles (Tips for battery, 2018). In this thesis, to be conservative, we estimate the lifetime to be 1,000 hours using 200 cycles.

The purchase cost of the charging equipment is assumed as \$1,500 based on the one of DJI charging equipment (Battery station, 2018). Referring to the warranty period (12 months) of this battery station (After-sales service policies, 2018), we assume the lifetime to be 5,000 hours.

The data transmission system parameters are estimated by referring to the data link systems used by UAV when implementing infrastructure inspection. The prices of two data link are \$700 (Bluetooth Datalink, 2018) and \$1,700 (Wireless UAV Data Link, 2018), so we assumed the price of the data transmission system as \$1,200. The lifetime is estimated according to the warranty period of 12 months of the system (After-sales service policies, 2018).

The auxiliary equipment typically consists of the industrial grade joystick, military grade monitor, CPU, video recorder and generator. The purchase costs of these equipment are estimated at \$300 for Industrial grade joystick products (Industrial grade joystick, 2018), \$800 for Military grade monitor products (Military grade monitor, 2018),

\$1,500 for CPU products (CPU, 2018), \$600 for Video recorder (Video recorder, 2018), and \$1,000 for Video generator products (Video generator, 2018), respectively. The warranty period of most of the equipment is around 12 months, which can be transferred to 5,000 hours in the utility industry.

The results of total cost comparison between two different power sources for the four scenarios are illustrated in Table 3-4. Compared to the lithium battery, the fuel cell can lead to a much higher cell depreciation cost as well as a much lower salary and setup cost. Except for the cell purchasing cost, the total cost of a fuel cell includes the fuel tank depreciation cost and refueling cost, which leads to a higher depreciation cost than a lithium battery. On the other side, due to a much lower total inspection time, the costs of salary, setup, data transmission system and auxiliary instruments depreciation are lower. Also, UAV powered by fuel cell has a lower maximum flying velocity, which is positively related to the total working time. It results in a little higher depreciation cost for the UAVs powered by a fuel cell. Since the contribution of battery or cell depreciation is much lower than that of the salary and setup cost, the total cost of UAV powered by the fuel cell is about 20% lower than by lithium battery.

In addition, in Table 3-5 and Figure 3-6, we compare the total cost of using a suspended robot in a 6-mile inspection distance with the total cost of UAV in 10 km (approximately 6 miles) inspection distance. It can be seen that the total cost can be reduced about 40%~50% by using UAV compared to the scenario of using a suspended robot (Nagarajan et al., 2017). Apparently, the salary cost decrement results in the major decrement of the total cost.

Table 3-4. Total Cost of UAV for inspection

	Lithium battery				Fuel cell			
Cost items	10km	30km	38km	45km	10km	30km	38km	45km
Salary	377.30	816.89	961.23	1,146.60	289.31	605.43	763.38	855.65
Setup	122.00	258.00	292.00	360.00	54.00	88.00	122.00	122.00
Battery/Cell depreciation	3.14	3.67	3.88	4.10	10.43	21.30	31.65	31.95
Data Transmission system depreciation	0.71	1.84	2.20	2.70	0.46	1.24	1.64	1.86
Auxiliary Equipment depreciation	2.00	5.16	6.17	7.50	1.30	3.47	4.59	5.20
Ground Travel	70.00	210.00	266.00	315.00	70.00	210.00	266.00	315.00
UAV depreciation	3.52	10.56	13.37	15.80	4.17	12.50	15.83	18.75
Total Cost (\$)	578.67	1,306.12	1,544.85	1,851.70	429.67	941.94	1,205.08	1,350.40

Table 3-5. Cost Decrement Table of the Suspended Robot and UAV

	Suspended Robot	UAV powered by a lithium battery	Decrement (%)	Suspended Robot	UAV powered by a hydrogen fuel cell	Decrement (%)
Cost items	6mile (9.66km)	10km		6mile (9.66km)	10km	
Salary cost (\$)	779.72	377.30	-52%	779.72	289.31	-63%
Other Cost (\$)	193.46	201.38	4%	193.46	140.36	-27%
Total Cost (\$)	973.18	578.67	-41%	973.18	429.67	-56%

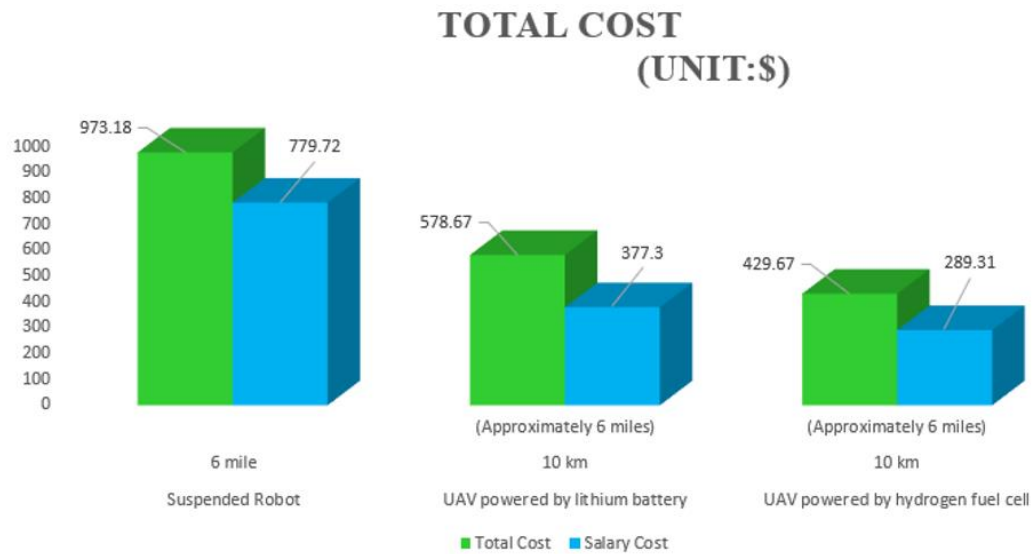


Figure 3-6. Cost Decrement Chart of the Suspended Robot and UAV

3.4. CONCLUSION

In this section, we investigate the routing algorithm and proposed the cost model for applications of UAVs in transmission line inspection considering both the lithium battery and the hydrogen fuel tank. The results of the case study show that when using UAVs for transmission line inspection, a significant decrease in the total cost can be achieved by reduction of the total inspection time, compared to suspended robots. Compared to the lithium battery system, hydrogen fuel cells can reduce the setup time, cost, and related salary expense, and thus achieve a better performance with respect to cost effectiveness.

4. ANALYTICAL MODEL

When we examined the results of the case study in Section 3, for the lithium battery-powered UAV, the number of battery replacement is the minimum since one battery cannot support the UAV as far as its communication distance. However, for the hydrogen fuel cell powered UAV, one fuel tank can support inspection distances that are longer than the communication distances. However, the ground team still needs to replace the fuel tank at every ground station when the remaining energy cannot support next inspection round. In this case, we intend to explore a better routing algorithm with a lower total cost. There is concern that some of the fuel tank replacements might be unnecessary if the flight radius is set to be variable value instead of a fixed value as proposed in Section 3. In other words, there is a minimum number of fuel tank replacements during the inspection trip, which is dependent on the inspection distance and the maximum feasible inspection distance. This number may be less than the total number of ground station deployment. An optimal combination of ground station deployments and fuel tank replacement when using UAV in transmission line inspection can be identified.

In this section, an analytical routing algorithm is first proposed to find the locations for the ground team deployment and fuel tank replacement that can minimize the total inspection cost. PSO is used to solve the proposed model for a near optimal solution. A numerical case study is conducted to compare the result of this analytical routing algorithm and the heuristic algorithm proposed in Section 3.

4.1. ANALYTICAL ALGORITHM AND COST MODEL

The inspection flight of the UAV needs to be controlled by a control station when the UAV motion signals are transmitted, and the live stream of inspection results are received. Let D be the total distance of the inspection trip of a transmission line. Such a distance is discretized into m segmentations with equal length of μ . Let $i, i=0, 1, \dots, m$, be the indexes of the start points of these m segmentations. Let d_{max} be the maximum distance inspected by a UAV using one hydrogen fuel cell tank, and m_d be the number of such segmentations contained in d_{max} . Let r_{max} be the maximum flying distance within which the control signals can be transmitted between the ground station and the UAV, and m_r be the number of such segmentations contained in r_{max} .

As shown in Figure 4-1, the ground team needs to set up the apparatus of the inspection at the point where the ground station is deployed. The UAV will first take off from the deployed station and fly back covering the distance of f_i^l with the maximum flying velocity v_2 (step 1 in Figure 4-1) to reach the left ending point of the inspection trip controlled by the deployed station. Then, UAV will fly forward to conduct the inspection covering the distance of $f_i^l + f_i^r$ with the inspection velocity v_1 (step 2 in Figure 4-1) to reach the right ending point of the inspection trip controlled by the deployed station. Similarly, v_1 is less than v_2 . After the distance of $f_i^l + f_i^r$ is inspected, the UAV flies back and lands at the ground station with a velocity of v_2 (step 3 in Figure 4-1). Such a procedure is defined as an inspection round controlled by a given ground station. Once the inspection round by the current ground station is completed, the ground team will pack the apparatus and relocate the ground team to the next station with the average

motion velocity v_3 (step 5 in Figure 4-1). Here, the inspection distance is the length of the transmission line that is inspected. Based on the process specified by Figure 4-1, the actual flying distance is twice of the inspection distance. The main difference between this analytical algorithm and the heuristic algorithm proposed in Section 3 is that in this algorithm the flight radius, f_i^l and f_i^r are variable instead of the fixed value r in (1) in the heuristic algorithm.

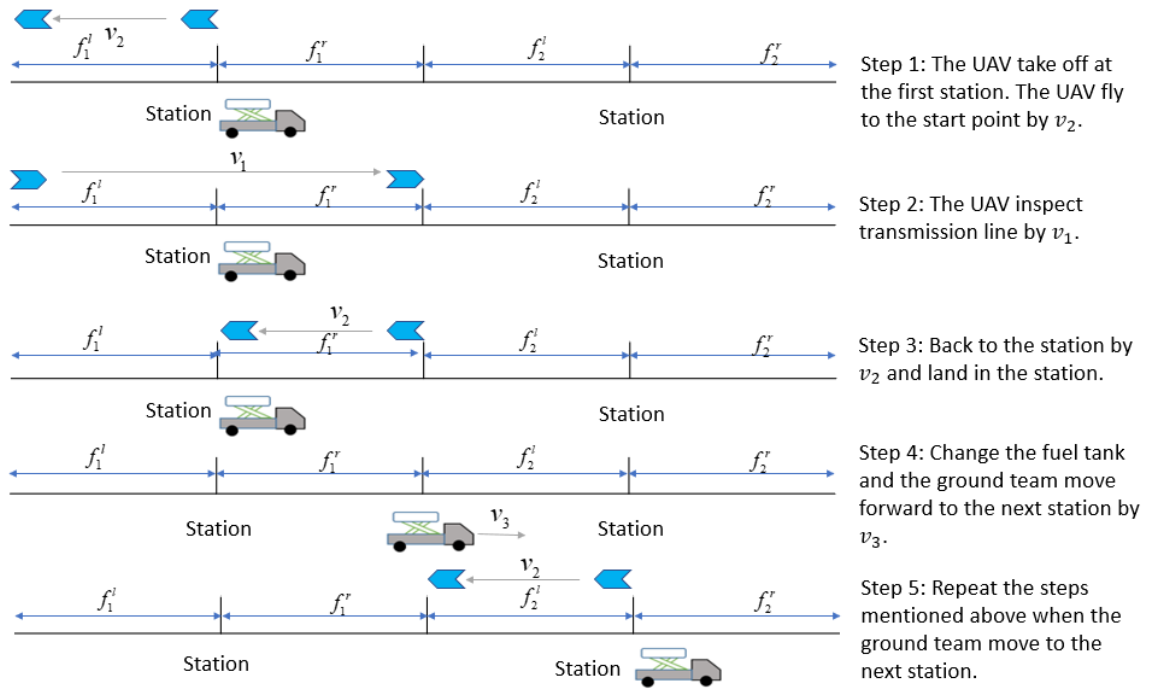


Figure 4-1. The Analytical General Method of the Inspection

Let x_i be the binary decision variable denoting if a ground station needs to be deployed at point i or not. Let y_i be the binary decision variable denoting if the fuel tank needs to be replaced or not at point i .

In the heuristic algorithm, we ignored the taking off and landing time of UAV. In order to solve the problem more accurately, the number of times for taking off and landing will be considered a new variable in this analytical algorithm. Let z_i be the decision variable denoting two different tank replacement strategies. It takes the value of two when the fuel tank is replaced after the left side inspection is covered. In this case, the UAV needs to take off and land for the left side, then, the UAV takes off and lands one more time for the right side. Otherwise, it takes the value of one if $x_i=1$, which can represent the cases 1) the fuel tank is replaced before the left side inspection, and 2) the fuel tank is not replaced (the landing and ground station deployment is only for the concern of data transmission range). When x_i is zero, then z_i is zero. Three different scenarios for the ground station power handling strategies while

$\{x_i = 1, y_i = 0, z_i = 1\}$, $\{x_i = 1, y_i = 1, z_i = 1\}$ and $\{x_i = 1, y_i = 1, z_i = 2\}$ are illustrated in Figure 4-2, Figure 4-3, and Figure 4-4, respectively.

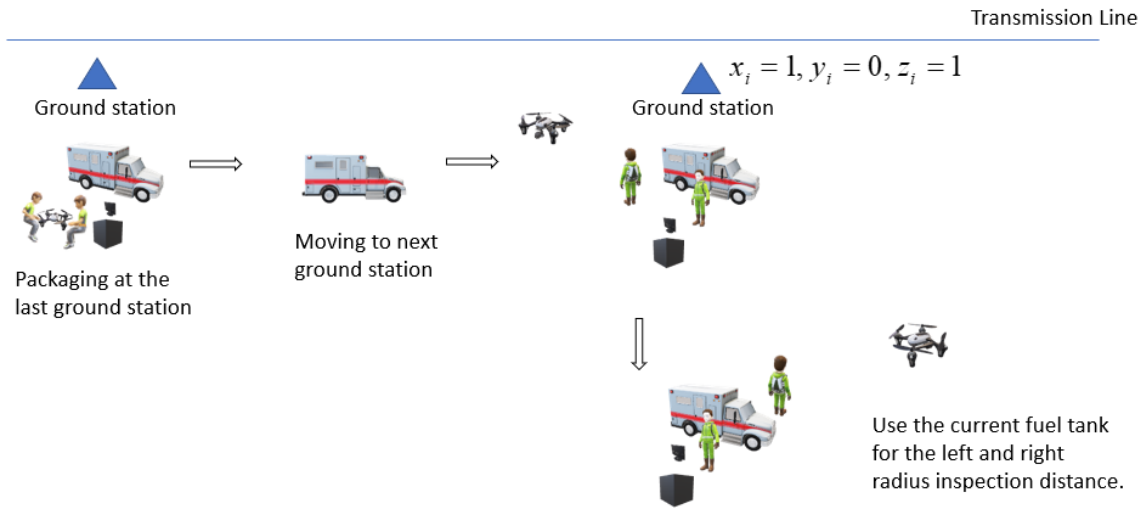


Figure 4-2. Ground Station Deployment & Relocation Scenario 1

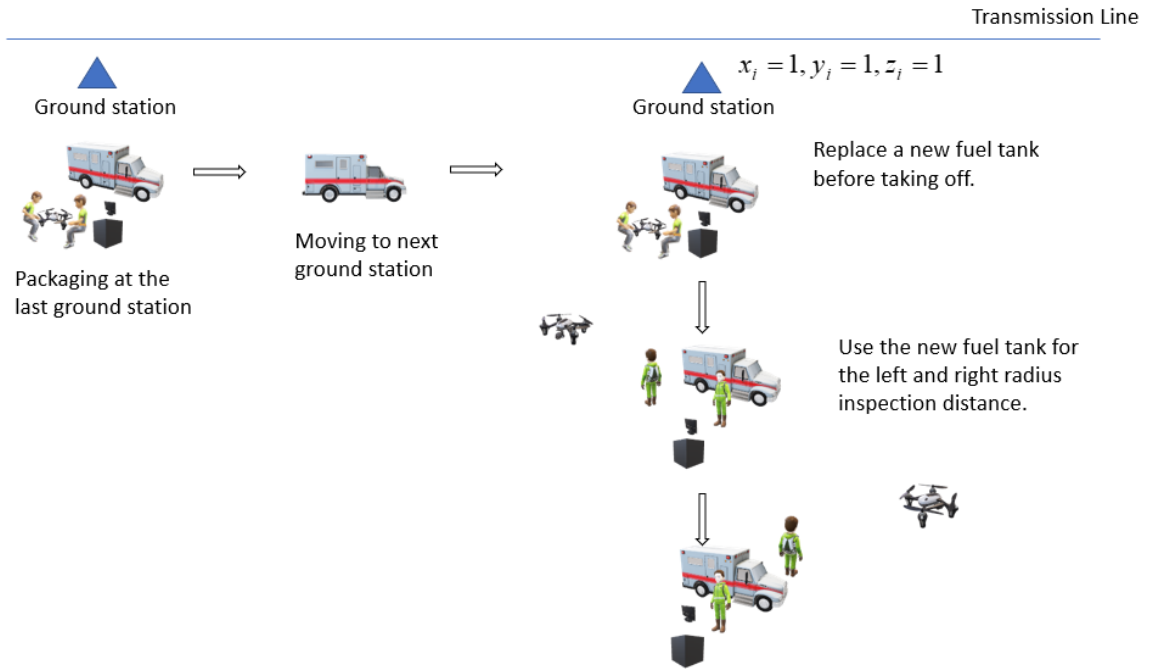


Figure 4-3. Ground Station Deployment & Relocation Scenario 2

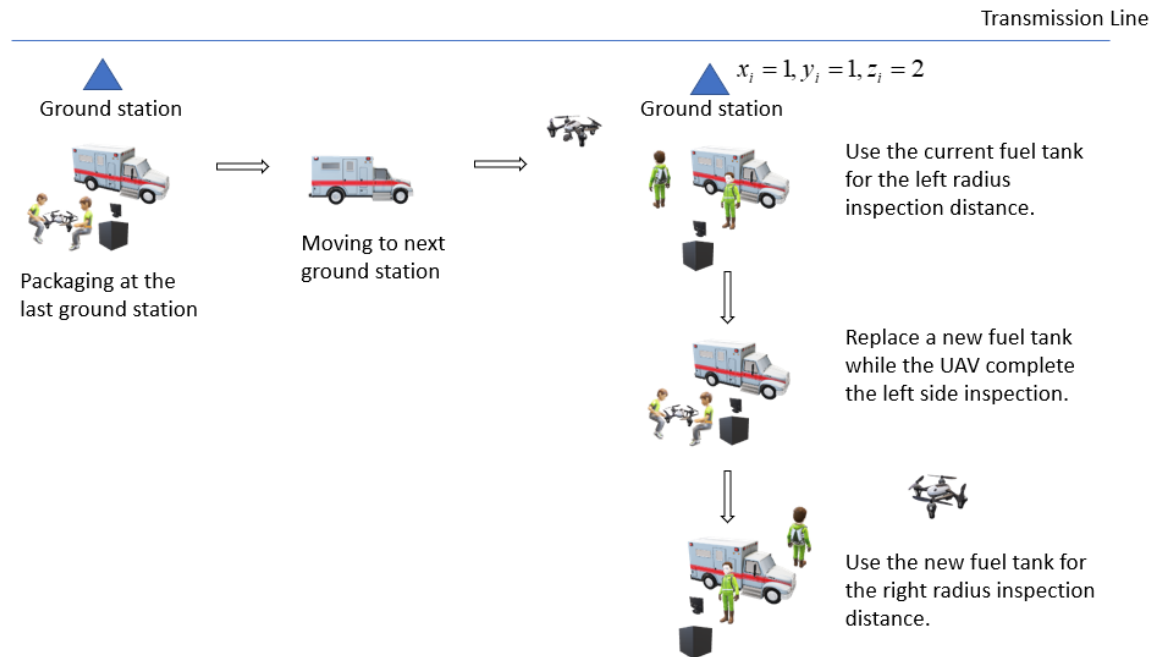


Figure 4-4. Ground Station Deployment & Relocation Scenario 3

The objective is to identify an optimal strategy in terms of the ground station deployment (i.e., x_i), fuel tank replacement (i.e., y_i, z_i), as well as the flying distances of the left and right sides of the inspection round controlled by each deployed ground station (i.e., f_i^l and f_i^r) to minimize the total inspection cost, which can be formulated by

$$\min_{x_i, y_i, z_i, f_i^l, f_i^r} TC = \min_{x_i, y_i, z_i, f_i^l, f_i^r} (C_{st} + C_s + C_{cd} + C_{dd} + C_{ud} + C_{ae} + C_{gt}) \quad (26)$$

where C_{st} , C_s , C_{cd} , C_{dd} , C_{ud} , and C_{gt} , denotes the salary cost for the inspection team, setup cost, depreciation cost of the fuel cell, depreciation cost of data transmission equipment, depreciation cost of UAV, depreciation cost of the auxiliary equipment, and the ground travel cost, respectively.

Salary cost C_{st} is formulated by:

$$C_{st} = (S_{dr} + 2S_{te})T_{Total} \quad (27)$$

where S_{dr} and S_{te} are the salary rates for the driver and the technicians in the ground team.

A typical inspection team consists of one driver and two technicians. T_{Total} is the total time for completing the inspection using UAV, which can be calculated by

$$T_{Total} = T_c + T_u + T_g + T_s \quad (28)$$

T_c is the final close time of the ground team when the inspection task is completed. T_u is the working time of the UAV, which can be calculated by

$$T_u = \frac{D}{v_1} + \frac{D}{v_2} + (t_{to} + t_{la}) \sum_{i=1}^m z_i \quad (29)$$

where t_{to} is the time required for one taking off of UAV. t_{la} is the time required for one landing of UAV. Note that $z_i=2$ will lead to one more additional landing and taking-off at point i where ground station is deployed, and the fuel tank is replaced.

T_g is the total travel time of the ground team, which can be calculated by

$$T_g = \frac{D}{v_3} \quad (30)$$

T_s is the total setup time of the ground team for relocation, which can be calculated by

$$T_s = t_{sg} \sum_{i=0}^m x_i + t_{sr} \sum_{i=0}^m y_i \quad (31)$$

where t_{sg} is the time required for a ground station setup after relocation. t_{sr} is the time required for a fuel tank replacement. Here we assume the station setup and the fuel tank replacement cannot be implemented simultaneously.

The setup cost, C_s , can be calculated by

$$C_s = C_{si} + c_{sg} \sum_{i=0}^m x_i + c_{sc} \sum_{i=0}^m y_i \quad (32)$$

where C_{si} is the cost of the initial setup to start the inspection task. c_{sc} is the cost required for one setup of fuel tank replacement. c_{sg} is the cost required for one setup of the ground team relocation.

The depreciation cost of the fuel cell, C_{cd} , can be calculated by

$$C_{cd} = G_h \sum_{i=0}^m y_i + G_t \frac{T_u}{L_t} + G_c \frac{T_u}{L_c} \quad (33)$$

where G_h is the cost of the refueling for each hydrogen fuel tank. G_t and G_c are the costs of hydrogen tank and hydrogen fuel cell, respectively. L_t and L_c are the expected lifetimes of tank and cell, respectively.

The depreciation cost of the data transmission system, C_{dd} , can be calculated by

$$C_{dd} = G_d \frac{T_u + T_s}{L_d} \quad (34)$$

where G_d is the purchase cost of the data transmission system. L_d is the expected lifetime of the data transmission system.

The depreciation cost of auxiliary equipment, c_{ae} , can be calculated by

$$C_{ae} = G_a \frac{T_u + T_s}{L_a} \quad (35)$$

where G_a is the cost of the auxiliary equipment. L_a is the expected lifetime of the auxiliary equipment.

The depreciation cost of UAV, C_{ud} , can be calculated by

$$C_{ud} = G_u \frac{T_u}{L_u} \quad (36)$$

where G_u is the cost of the UAV. L_u is the expected lifetime of the UAV.

The cost incurred by ground travel, c_{gt} , can be formulated by

$$C_{gt} = c_{gt} D \quad (37)$$

where c_{gt} is the ground travel cost per unit distance.

The constraints are formulated as follows. Since r_{max} is the maximum flying distance to guarantee the data transmission between UAV and ground station, there needs at least one ground station deployed in the distance of $2r_{max}$, to ensure the ground team can receive the signals transmitted by UAV, which can be formulated by

$$\sum_{i=k}^{k+2m_r-1} x_i \geq 1, \quad \forall k \in A = (-m_r, m-m_r] \quad (38)$$

Note that in (38), m_r virtual points are added before point x_0 and after point x_m , respectively, as shown in Figure 4-5 to make sure there should be at least one ground station deployed in the first and the last r_{\max} distance.

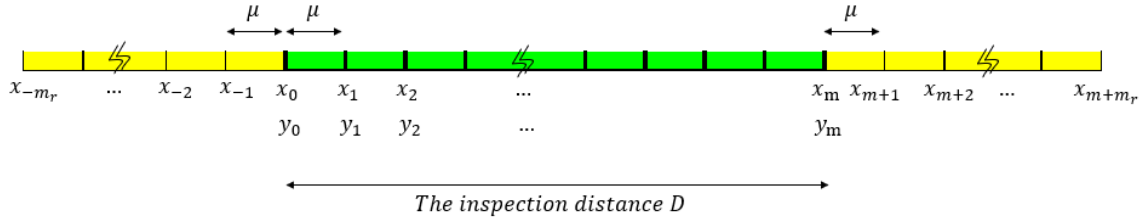


Figure 4-5. Virtual Points

The auxiliary points will not be considered for ground station deployment, which can be represented by

$$x_i = 0, \forall i \in \{-m_r, \dots, 0, \dots, m, m+1, \dots, m+m_r\} \quad (39)$$

The fuel tank cannot be replaced at point i at which the ground station is not deployed, which can be formulated by

$$y_i - x_i \leq 0 \quad \forall i \in [0, m] \quad (40)$$

The z_i can only take the value of zero when x_i is zero, which can be formulated by

$$z_i = 0, \text{ if } x_i = 0 \quad \forall i \in [0, m] \quad (41)$$

The z_i cannot take the value of two when y_i is zero, which can be formulated by

$$z_i \neq 2, \text{ if } y_i = 0 \quad \forall i \in [0, m] \quad (42)$$

There should be at least one replacement of fuel tank for every d_{\max} inspection distance, which can be formulated by

$$\sum_{i=k}^{\min(k+m_d-1, m)} y_i \geq 1, \quad \forall k \in [1, \max(1, m - m_d)] \quad (43)$$

It should be noted that the first ground station needs to be deployed within the first r_{max} distance. (i.e., it implies that a new fuel tank is mounted at the first ground station when inspection starts), which can be formulated by

$$\sum_{i=0}^{m_r} y_i \geq 1 \quad (44)$$

In addition, the total number of fuel tank replacement should be larger or equal to the number of minimum replacements which depends on the total inspection distance D and the maximal feasible inspection distance d_{max} . It can be formulated by

$$\sum_{i=0}^m y_i \geq \left\lceil \frac{D}{d_{max}} \right\rceil \quad (45)$$

The total number of the ground station deployment should be no less than the minimum required number, which can be formulated by

$$\sum_{i=0}^m x_i \geq \left\lceil \frac{D}{2r_{max}} \right\rceil \quad (46)$$

f_i^l and f_i^r are meaningless when there is no ground station deployed at point i ,

which can be formulated by

$$f_i^l = 0, \quad \text{if } x_i = 0 \quad (47)$$

$$f_i^r = 0, \quad \text{if } x_i = 0 \quad (48)$$

The sum of f_i^l and f_i^r should be the total inspection distance, which can be formulated by

$$\sum_{i=0}^m f_i^l + \sum_{i=0}^m f_i^r = m \quad (49)$$

Since r_{max} is the maximum flying distance to guarantee the data transmission between the UAV and the ground station, f_j^l and f_j^r are limited to the m_r , which can be formulated by

$$f_i^r \leq m_r \quad (50)$$

$$f_i^l \leq m_r \quad (51)$$

The inspection distance should be constrained by the fuel tank capacity, which can be formulated by

$$x_i d_i^l \leq m_d \quad (52)$$

$$x_i d_i^r \leq m_d \quad (53)$$

where d_i^l and d_i^r are the accumulated inspection distances covered by the current fuel tank upon the completion of the left and right sides inspection trips controlled by the ground station i . d_i^l and d_i^r can be calculated by

$$d_i^l = \begin{cases} f_i^l, & \text{if } x_i = 1, y_i = 1, z_i = 1 \\ d_{i-1}^r + f_i^l, & \text{if } x_i = 1, y_i = 0 \\ d_{i-1}^r + f_i^l, & \text{if } x_i = 1, y_i = 1, z_i = 2 \\ d_{i-1}^r, & \text{if } x_i = 0 \end{cases} \quad (54)$$

$$d_i^r = \begin{cases} f_i^l + f_i^r, & \text{if } x_i = 1, y_i = 1, z_i = 1 \\ f_i^r + d_i^l, & \text{if } x_i = 1, y_i = 0 \\ f_i^r, & \text{if } x_i = 1, y_i = 1, z_i = 2 \\ d_{i-1}^r, & \text{if } x_i = 0 \end{cases} \quad (55)$$

Initially, d_0^l and d_0^r are equal to 0.

When the ground team replaces a new fuel tank before the UAV takes off for its left side inspection trip ($x_i = 1, y_i = 1, z_i = 1$), d_i^l is equal to the left side flying distance controlled by the ground station i , while d_i^r is the sum of the left and right sides flying distance controlled by the ground station i .

When the ground team replaces the fuel tank after the left side inspection of the ground station deployed at the point i is completed, i.e., uses the last fuel tank for the left radius and replaces a new tank for the right radius of the ground station at point i ($x_i = 1, y_i = 1, z_i = 2$), d_i^l is the sum of d_{i-1}^r and the left radius f_i^l of the point i , while d_i^r is equal to f_i^r .

When the fuel tank is not replaced at the station deployed at point i ($x_i = 1, y_i = 0$), d_i^l is the sum of d_{i-1}^r and the left radius f_i^l of the point i , while d_i^r is the sum of d_i^l and f_i^r .

4.2. SOLUTION STRATEGY BASED ON PSO

In PSO, the particle is encoded as follows

$$p = [x_0, \dots, x_m, y_0, \dots, y_m, z_0, \dots, z_m, f_0^l, \dots, f_m^l, f_0^r, \dots, f_m^r] \quad (56)$$

The fitness function of each particle can be formulated by (57) where the constraints (38)-(53) are integrated as penalty terms.

$$\begin{aligned}
& TC + A \cdot [\min(\sum_{i=\alpha}^{\alpha+2m_r-1} x_i - 1, 0)]^2 + A \cdot [\min(x_\beta, 0)]^2 + A \cdot [\min(x_i - y_i, 0)]^2 \\
& + A \cdot [\min(A \cdot x_i - z_i, 0)]^2 + A \cdot [\min(1 - z_i + y_i, 0)]^2 + A \cdot [\min(\sum_{i=\mu}^{\mu+m_d-1} y_i - 1, 0)]^2 \\
& + A \cdot [\min(\sum_{i=0}^{m_r} y_i - 1, 0)]^2 + A \cdot [\min(\sum_{i=0}^m y_i - \left\lceil \frac{D}{d_{\max}} \right\rceil, 0)]^2 + A \cdot [\min(\sum_{i=0}^m x_i - \left\lceil \frac{D}{2r_{\max}} \right\rceil, 0)]^2 \\
& + A \cdot [\min(A \cdot x_i - f_i^l, 0)]^2 + A \cdot [\min(A \cdot x_i - f_i^r, 0)]^2 + A \cdot [\sum_{i=0}^m f_i^l + \sum_{i=0}^m f_i^r - m]^2 \\
& + A \cdot [\min(m_r - f_i^l, 0)]^2 + A \cdot [\min(m_r - f_i^r, 0)]^2 + A \cdot [\min(d_{\max} - x_i d_i^l, 0)]^2 \\
& + A \cdot [\min(d_{\max} - x_i d_i^r, 0)]^2, \forall i \in [0, m], \forall \beta \in \{-m_r, \dots, 0, m+1, \dots, m+m_r\}, \\
& \forall \alpha \in (-m_r, m-m_r), \forall \mu \in [1, \max(1, m-m_d)]
\end{aligned} \tag{57}$$

where A is a large real number.

It can be seen from (56), the dimension of p is $5(m+1)$. As mentioned earlier, the total inspection distance D is discretized into m segmentations with equal length of μ . To facilitate a high resolution of the model, μ can take very small values, and thus, m and the dimension of each particle could be very high. PSO may be awkward when handling the high dimension particles.

To reduce the dimension of the particle in PSO, we consider the strategy of the minimal ground station deployment. Since the largest distance between two ground stations is $2r_{\max}$, also recall that the flying radius by one fuel tank is larger than the flying radius determined by the data transmission, the minimal number of the ground stations can be calculated as follows:

$$N_x = \left\lceil \frac{m}{2m_r} \right\rceil \tag{58}$$

Let $j, j=1, 2, \dots, N_x$, be the index of locations where the ground team can be deployed according to the minimal deployment specified by (58). In this case, x_j, y_j, z_j, f_j^l , and f_j^r need to be identified. Thus, the dimension of each particle can be reduced

from $5(m+1)$ to $4N_x$. For example, if $m=150$, $m_r=40$, then $N_x=2$, the dimension of the particle will be reduced from 755 to 8 as illustrated in Figure 4-6.

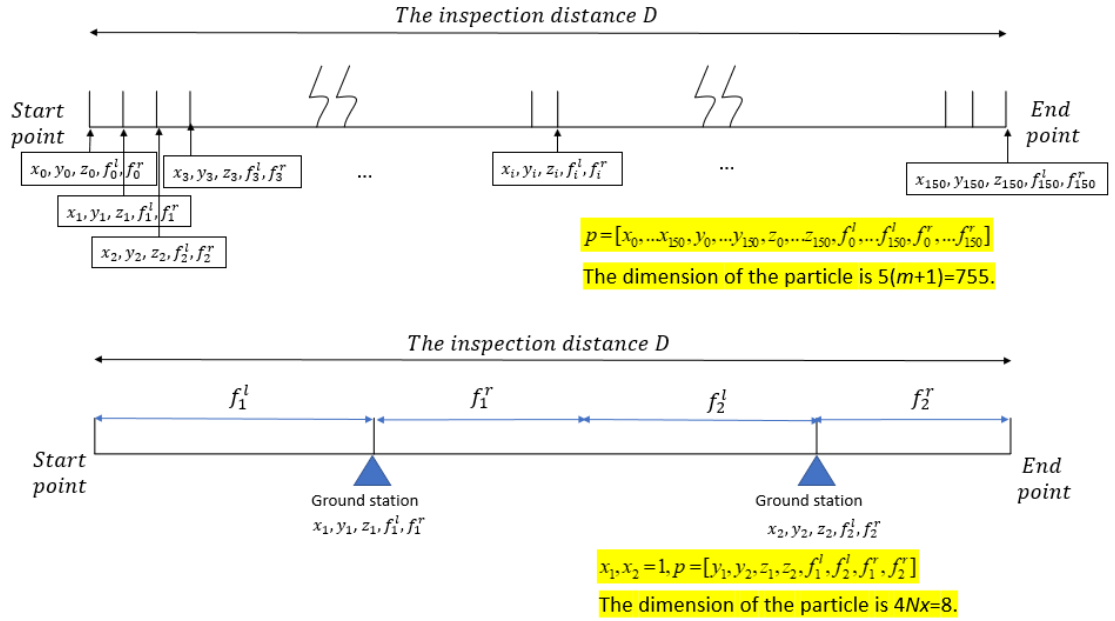


Figure 4-6. Particle Dimension Reduction Example

The constraints of (38) - (41), (43) and (46) - (48) could be ignored in PSO. We set $y_1=1$ instead of (44) to ensure that a new fuel tank is mounted at the first ground station. For each ground station, the UAV needs to take off and land at least once, it can be presented as:

$$z_j \in \{1, 2\}, \quad \forall j \in [1, N_x] \quad (59)$$

Here, we stipulate that UAV uses the new fuel tank to complete the inspection of the left and right side of the first ground station. Thus, $z_1=1$.

(54) and (55) can be revised accordingly as follows:

$$d_j^l = \begin{cases} f_j^l, & \text{if } y_j = 1 \text{ and } z_j = 1 \\ d_{j-1}^r + f_j^l, & \text{if } y_j = 0 \\ d_{j-1}^r + f_j^l, & \text{if } y_j = 1 \text{ and } z_j = 2 \\ d_1^l = f_1^l \end{cases} \quad (60)$$

$$d_j^r = \begin{cases} f_j^l + f_j^r, & \text{if } y_j = 1 \text{ and } z_j = 1 \\ f_j^r + d_j^l, & \text{if } y_j = 0 \\ f_j^r, & \text{if } y_j = 1 \text{ and } z_j = 2 \end{cases} \quad (61)$$

The minimal number of fuel tank replacements is Min_N_y . Since each fuel tank can support d_{max} inspection at most, Min_N_y can be calculated as follows:

$$Min_N_y = \left\lceil \frac{D}{d_{max}} \right\rceil \quad (62)$$

If N_y is equal to Min_N_y , we do not need to use PSO to explore a better solution since the number of fuel tank replacement achieves the minimum value.

If N_y is larger than Min_N_y , we need to explore a better solution with respect to the number of fuel tank replacement from Min_N_y to N_y . Let $check_NY$ be the variable to denote each possible number of fuel tank replacement within this range. It can be formulated as

$$check_NY \in [Min_N_y, N_y] \quad (63)$$

Thus, constraint (45) can be modified to

$$\sum_j y_j = check_N_y \quad (64)$$

We examine different values of $check_NY$ from Min_N_y . The algorithm will be terminated if a feasible solution with the current $check_NY$ can be obtained. Otherwise, the $check_NY$ will be updated by adding one until it equals to N_y .

The fitness function of individual particle can be revised as shown in (65) where the constraints (42), (44), (49)-(53), (59) and (64) are integrated as penalty terms:

$$\begin{aligned}
 & TC + A \cdot [\min(1 - z_j + y_j, 0)]^2 + A \cdot [\min(y_1 - 1, 0)]^2 + A \cdot [\min(z_1 - 1, 0)]^2 \\
 & + A \cdot \left[\sum_{j=1}^{N_x} f_j^l + \sum_{j=1}^{N_x} f_j^r - m \right]^2 + A \cdot [\min(m_r - f_j^l, 0)]^2 + A \cdot [\min(m_r - f_j^r, 0)]^2 \\
 & + A \cdot [check_NY - \sum_{j=1}^{N_x} y_j]^2 + A \cdot [\min(d_{max} - d_j^l, 0)]^2 + A \cdot [\min(d_{max} - d_j^r, 0)]^2
 \end{aligned} \tag{65}$$

In PSO, the particles fly in the search space based on the updated velocity towards the best location of both itself and entire swarm over time. After each iteration, the velocity of each particle is updated according to (66).

$$v(q+1) = v(q) \times w + c_1 \times \alpha_1 \times (p_{best} - p(q)) + c_2 \times \alpha_2 \times (g_{best} - p(q)) \tag{66}$$

where w is inertia weight, c_1 and c_2 are acceleration coefficients, α_1 and α_2 are random real numbers between zero and one, respectively. In addition, $v(q)$ and $p(q)$ are the matrices of the velocity and location of individual particle at iteration q . p_{best} is the particle's best location that has been identified up to the q^{th} iteration and g_{best} is the global best location of the entire swarm. The location of each particle is updated according to (67).

$$p(q+1) = p(q) + v(q+1) \tag{67}$$

The procedure of the algorithm has been illustrated in a flowchart as shown in Figure 4-7 and briefly described as follows.

1. Calculate N_x and N_y , i.e., the number of ground station deployments and the number of cell tank replacements based on the heuristic algorithm.
2. Calculate Min_N_y using (62).
3. Terminate the algorithm if N_y is equal to Min_N_y .
4. Otherwise, let Min_N_y be $check_NY$ and using PSO algorithm to search a better solution.
 - 4.1. Randomly initialize the parameters and form a swarm.
 - 4.2. Calculate the fitness for each particle using (65).
 - 4.3. Start the PSO algorithm.
 - 4.3a. Update the velocity for each particle using (66).
 - 4.3b. Update the location for each particle using (67).
 - 4.3c. Update the particle best and global best if necessary.
 - 4.3d. If the iteration is maximum:
 - 4.3d.1. Terminate the algorithm.
 - 4.3d.2. Terminate the algorithm and adopt the global best result as the optimal deployment, if the best result of the PSO is feasible.
 - 4.3d.3. Terminate the algorithm and adopt the deployment based on the heuristic algorithm, if the best result of the PSO is infeasible and $check_NY$ is equal to N_y .
 - 4.3d.4. Let $check_NY = check_NY + 1$ and repeat step 4.1, if the best result of the PSO is infeasible and $check_NY$ is not equal to N_y .

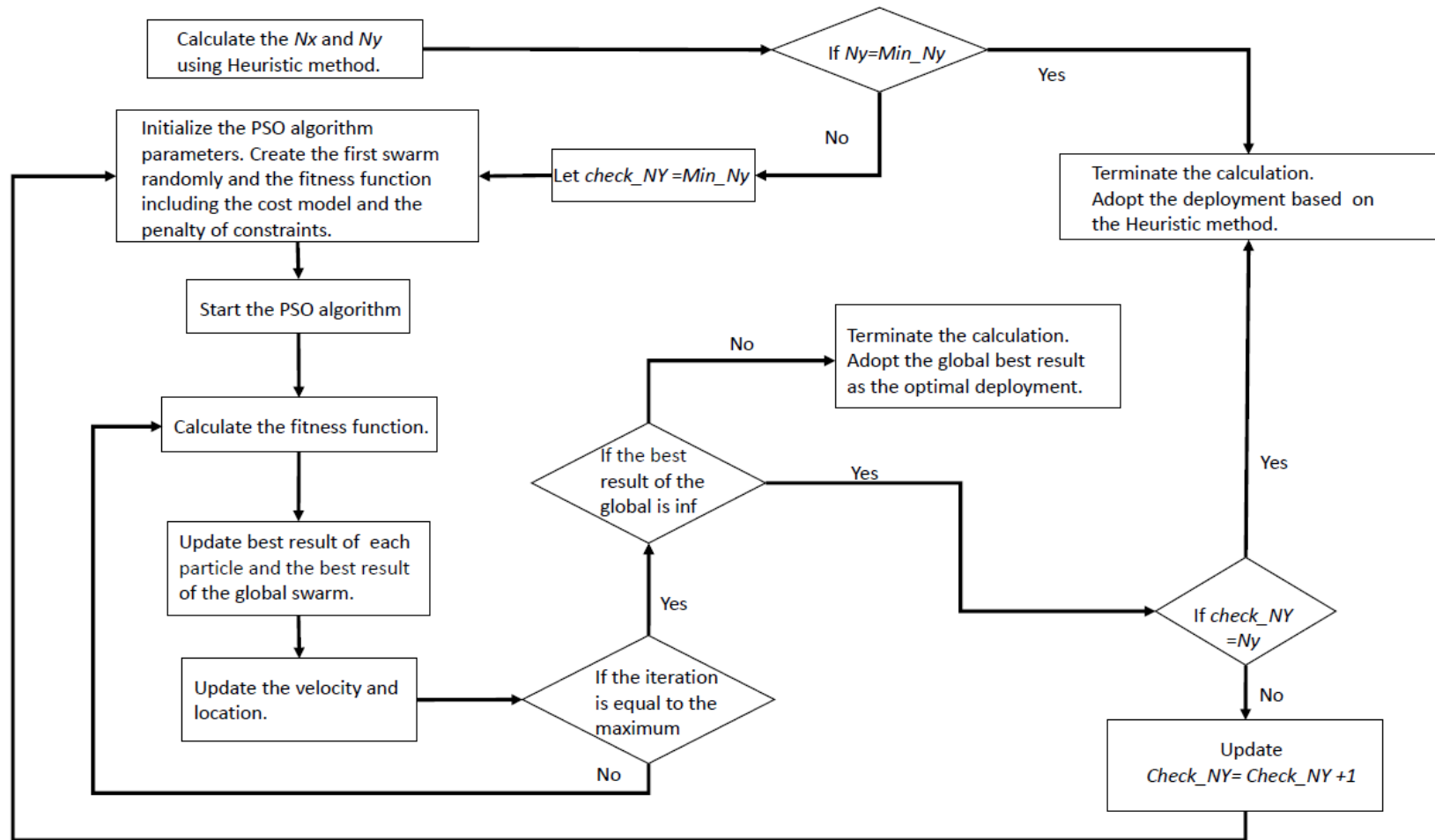


Figure 4-7. Flowchart of the Analytical Algorithm

4.3. CASE STUDY

In this section, we calculate the number of the ground station deployments and the fuel tank replacements based on the heuristic and analytical methods. The total costs based on two different methods for inspecting five different distances (10 km, 30 km, 38 km, 45 km, 50 km) are obtained and analyzed.

The times required for taking off t_{to} and landing t_{la} are the new parameters in the analytical method. Assumed t_{to} and t_{la} are both equal to 2 min. Other parameters are the same as the ones used in Section 3.3.

Matlab is used to run the proposed PSO algorithm for solving the problem. The parameters used in the PSO algorithm are listed in Figure 4-8.

```
%% set the parameters of the pso algorithm
N = 500;                % initialize the number of the population
d = 4*Nx;               % dimation of each particle
max_iter = 5000;        % maximum number of iterations
w = 0.8;                % inertia weight
c1 = 1.5;               % acceleration coefficients
c2 = 1.5;               % acceleration coefficients
```

Figure 4-8. Parameters of PSO Algorithm

The results are compared in Table 4-1. Note that, in order to make the comparison based on a same baseline, the taking off and landing times are added to the heuristic algorithm in calculation. It can be seen that for the cases of 10km, 30km and 45km, due to the fuel tank replacement calculated by the heuristic algorithm is the minimal number of fuel tank replacement, there is no reduction for total time and cost when using the analytical algorithm. However, for 38km and 50km, the fuel tank

replacement calculated by the heuristic algorithm is not the minimal value. In this case, the better solution is identified by using the analytical model.

Table 4-1. Comparison Result of Two Method

		Ground stations (Unit: No.)	Fuel tank replacement (Unit: No.)	Total time (Unit: hr)	Total cost (Unit: \$)
10 km	Method 1	1	1	2.8220	437.29
	Method 2	1	1	2.8220	437.29
30 km	Method 1	2	2	5.8994	956.17
	Method 2	2	2	5.8994	956.17
38 km	Method 1	3	3	7.4703	1,226.13
	Method 2	3	2	7.3703	1,188.94
45 km	Method 1	3	3	8.3490	1,371.33
	Method 2	3	3	8.3490	1,371.33
50 km	Method 1	4	4	9.5434	1,579.06
	Method 2	4	3	9.4434	1,541.87

*Method 1: Heuristic method; Method 2: Analytical method;

The comparison of the ground station deployment and power system replacement is illustrated in Figure 4-9 and Figure 4-10.

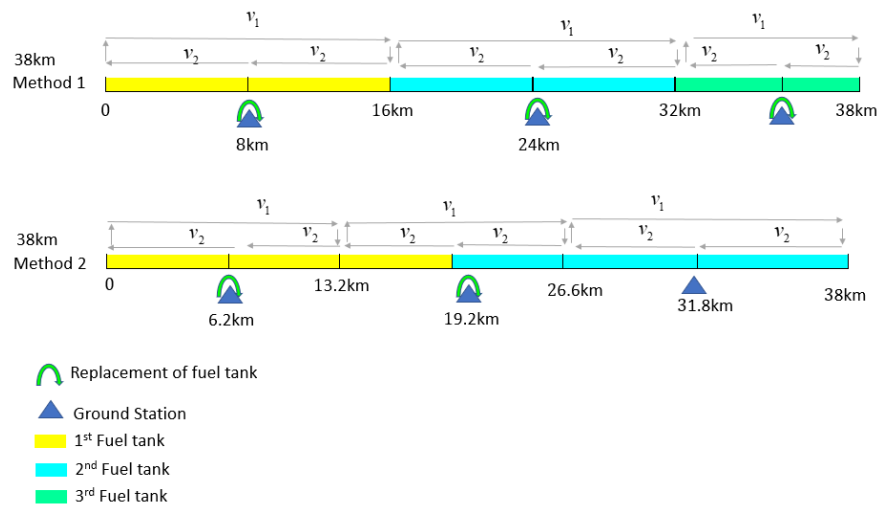


Figure 4-9. Deployment and Replacement Comparison of 38km



Figure 4-10. Deployment and Replacement Comparison of 50km

We also compare the transmission line inspection cost and time per kilometer in Figure 4-11 - Figure 4-15. The unit performance of the analytical algorithm and heuristic algorithm for the fuel cell system is based on the result of the 38km inspection distance of the case study in this section. The unit performance of the heuristic algorithm for the lithium battery system is based on the result of the 38km inspection distance of the case study in Section 3. The unit performance of the suspended robot is based on the cost of low frequency obstacle of 30mile, which is approximately equal to 50km in (Nagarajan et al., 2017).

Figure 4-11 and Figure 4-12 show the comparisons of unit time and unit cost. Obviously, both unit time and cost of using a suspended robot are much higher than UAV. It's mainly because of the low velocity of the suspended robot and the long time spent in clearing obstacles.

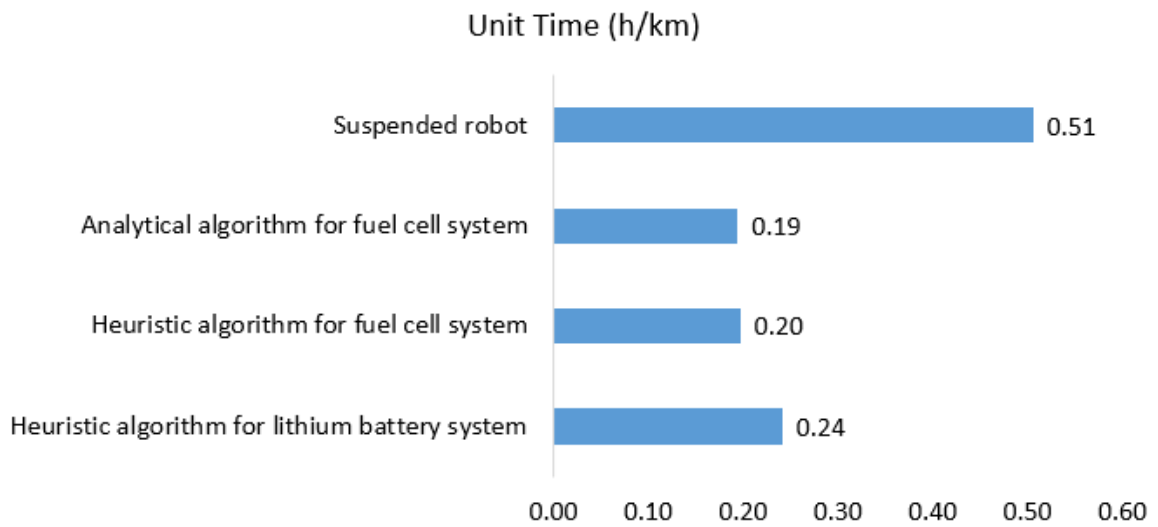


Figure 4-11. Comparison of Unit Time

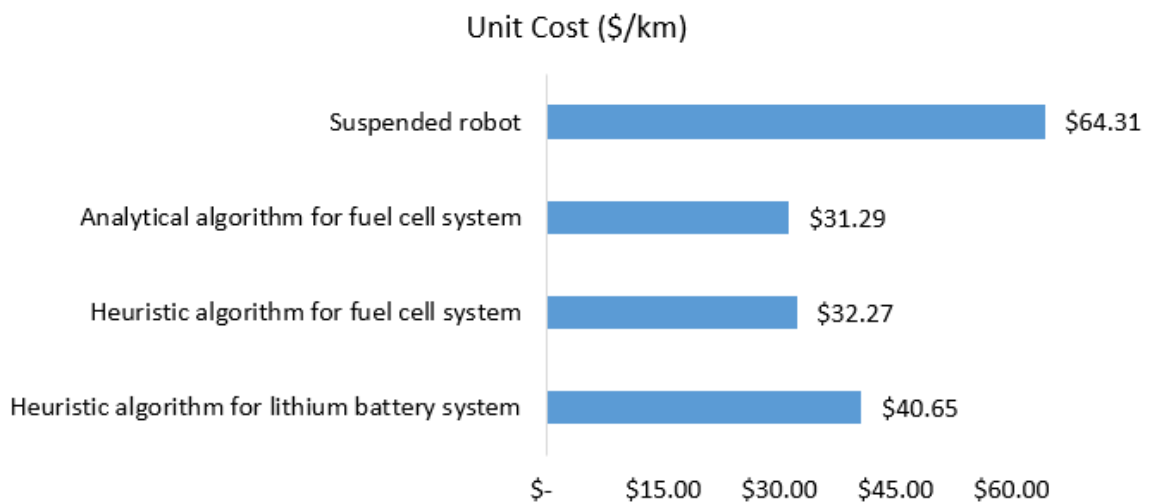


Figure 4-12. Comparison of Unit Cost

Figure 4-13 shows the comparison of unit salary cost. The salary cost is the main component of the total cost. Similarly, the unit salary cost of a suspended robot is higher than UAV.

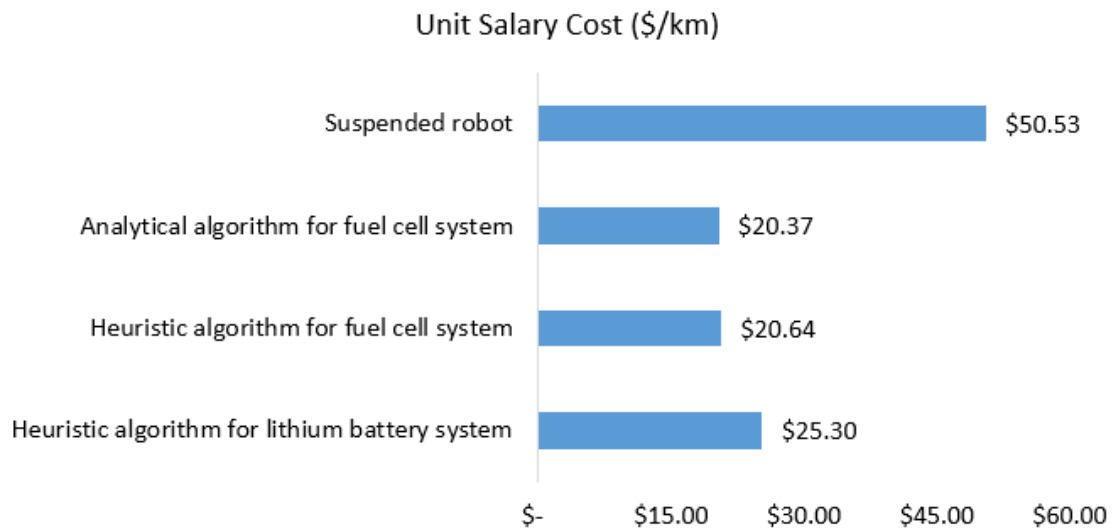


Figure 4-13. Comparison of Unit Salary Cost

Figure 4-14 shows the comparison of unit setup cost. Unlike the unit time, unit cost, and unit salary cost, the unit setup cost of using UAV with a lithium battery system is the highest among all the options. This is because the capacity of lithium battery is limited and unable to support UAV for a long flying distance. Thus, the battery needs to be replaced frequently so that the inspection can be completed, which leads to a high setup cost.

Figure 4-15 shows the comparison of unit battery or cell depreciation cost. Due to the high cost of the fuel cell system, the unit cell depreciation cost is higher than the suspended robot and the UAV with the lithium battery system. However, it needs to be noted that the depreciation cost accounts for a small part of the total cost when using either a fuel cell or a lithium battery.

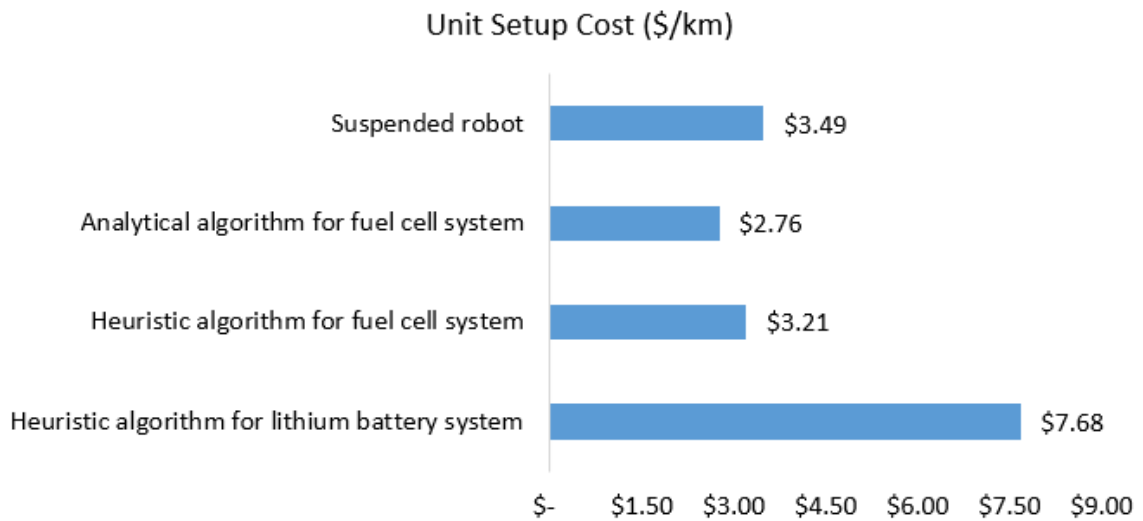


Figure 4-14. Comparison of Unit Setup Cost

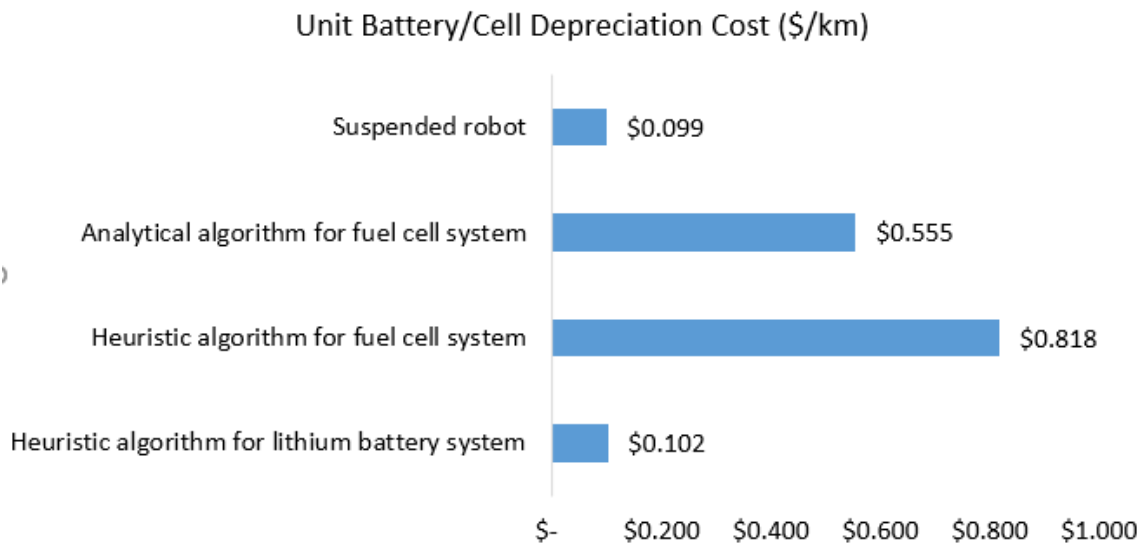


Figure 4-15. Comparison of Unit Battery/Cell Depreciation Cost

4.4. CONCLUSION

In this section, the heuristic routing model was advanced to an analytical one to further improve the cost-effectiveness of the transmission line inspection using a UAV. A

PSO-based optimization algorithm was proposed to solve the analytical model for identifying a better strategy for ground station deployment and power system replacement. We compared the unit cost of the transmission line inspection when using suspended robot, UAV with lithium battery power system based on the heuristic model, and UAV with fuel cell power system based on both heuristic and analytical models. Based on unit inspection distance, when measured with the analytical model, the performance of UAV with a fuel cell power system is superior to the other options.

5. CONCLUSIONS

In this thesis, we investigated the routing algorithm and implemented cost-effectiveness analysis for the applications of the UAVs in transmission line inspection. Both heuristic and analytical models were proposed for the routing algorithm to identify the locations for the ground station deployment and power system replacement. The results of the case study based on both algorithms show that using UAVs for transmission line inspection will lead to a significant decrease of the total cost compared when suspended robots are used.

Although the applicability looks very specific based on the case study illustrated in this thesis, the contribution in terms of applications is not trivial. First, the method can be used in many other applications with similar concerns after necessary and limited revisions. For example, with the rapid development of UAV technology, UAVs have been used for many areas, such as agriculture, filmmaking, etc. Almost all tasks conducted by UAVs need to consider the tradeoff between the number of ground station deployment sites and the capacity of the power system.

For future work, the sensitivity of the cost with respect to other factors will be analyzed. For instance, the potential risk cost for the flammability of hydrogen, the cost of usage deterioration of the lithium battery, and the decreased cost of reusing the hydrogen tank after activating treatment rather than using a new one could be investigated.

BIBLIOGRAPHY

- After-sales service policies, 2018. Available at: <https://www.dji.com/service/policy>
- Alvear, O., Calafate, C.T., Zema, N.R., Natalizio, E., Hernández-Orallo, E., Cano, J.C. Manzoni, P., 2018. A Discretized Approach to Air Pollution Monitoring Using UAV-based Sensing. *Mobile Networks and Applications*, 23(6), pp.1693-1702.
- Alvear, O., Zema, N.R., Natalizio, E. and Calafate, C.T., 2017, June. A chemotactic pollution-homing UAV guidance system. In *Wireless Communications and Mobile Computing Conference (IWCMC), 2017 13th International* (pp. 2115-2120). IEEE.
- Asakawa, K., Kojima, J., Kato, Y., Matsumoto, S., Kato, N., Asai, T., Iso, T., 2012. Design concept and experimental results of the autonomous underwater vehicle aqua explorer 2 for the inspection of underwater cables. *Advanced Robotics journal*. 16(1), 27-42.
- Bagheri, A., Peyhani, H. M., Akbari, M., 2014. Financial forecasting using ANFIS networks with quantum-behaved particle swarm optimization. *Expert Systems with Applications*, 41(14), 6235-6250.
- Bastian, N.D., Trainor, T.E., 2010. Going green at west point: is it economically beneficial? A cost-benefit analysis of installing a wind farm at the united states military academy. *Engineering Management Journal*. 22(3), 12-20.
- Battery station, 2018. Available at: <https://store.dji.com/product/inspire-2-battery-station>
- Bluetooth Datalink, 2018. Available at: <https://store.dji.com/product/a2-iosd-mark-ii-2-4g-bluetooth-datalink?from=search-result-v2&position=27>
- Candido, S., Kim, Y.T., Hutchinson, S., 2008. An improved hierarchical motion planner for humanoid robots. *IEEE-RAS International Conference on Humanoid Robots*. 654–661. Daejeon, Korea.
- Carrabs, F., Cerulli, R., Speranza, M.G., 2013. A branch-and-bound algorithm for the double travelling salesman problem with two stacks. *Networks*, 61(1), 58-75.
- Chen, Z., Xiong, R., Cao, J., 2016. Particle swarm optimization-based optimal power management of plug-in hybrid electric vehicles considering uncertain driving conditions. *Energy*, 96, 197-208.
- Cosio, F.A., Castaneda, M.A.P., 2004. Autonomous robot navigation using adaptive potential fields. *Mathematical and Computer Modelling*. 1141-1156.

- CPU, 2018: (1) Available at: <https://www.ebay.com/p/1pc-Siemens-PLC-Module-6es7-314-6ch04-0ab0-One-Year/2255315779?iid=401681850793&chn=ps> (2) Available at: https://www.plchardware.com/Products/SM-6ES7314-6CH04-0AB0-NSS.aspx?gclid=CjwKCAiAsoviBRAoEiwATm8OYJ_oXEoIjHl-7q5lVeC4Inu_GWz4fy1F2v46Gl2CVJhtPmbIn8SohoCls8QAvD_BwE Industrial grade joystick, 2018: (1) Available at: https://www.walkerindustrial.com/MKTB32-WKT-26-Schmersal-Accessories-Industrial-Gra-p/MKTB32-WKT-26.htm?gsn&gclid=CjwKCAiAsoviBRAoEiwATm8OYC6aByEINCa9xjllSJbqGCsWLCJtAC_RDcI9eevJ3CrK39u1B1q6SBoCkJ4QAvD_BwE (2) Available at: http://shop.itacsystems.com/products/joystick-j538bb13.html?gclid=CjwKCAiAsoviBRAoEiwATm8OYEAcNw5JdUQ37owvnj6Yu2RW5gUAjWzjy90XwCczgGHfI0MXVBzGRoCYeEQAvD_BwE
- DOE, 2017. Available at: <https://www.energy.gov/eere/fuelcells/doe-technical-targets-on-board-hydrogen-storage-light-duty-vehicles>
- DJI website: The graphic of payload and flight time. Retrieved from the DJI company- Available at: <https://www.dji.com/matrice-200-series/payloads#subNavBar>
- Earp G., Eyre-Walker R., Ellam A. and Thomas A., 2011. Advanced aerial inspection and asset management of electricity towers. *Proceedings of IEEE PES International Conference on Transmission and Distribution Construction, Operation and Live-line Maintenance*. 2011, pp.1-7.
- Eberhart, R., Kennedy, J., 1995. A new optimizer using particle swarm theory. In *Micro Machine and Human Science, 1995. MHS'95., Proceedings of the Sixth International Symposium on* (pp. 39-43). IEEE.
- Elizondo, D., Gentile, T., Candia, H., Bell, G., 2010. Overview of robotic applications for energized transmission line work –technologies, field projects and future developments. *Proceedings of 2010 1st International Conference on Applied Robotics for the Power Industry Delta Centre-Ville Montréal, Canada*. October 5-7.
- Fiechter, C.N., 1994. A parallel tabu search algorithm for large traveling salesman problems. *Discrete Applied Mathematics*, 51(3). 243-267.
- Foudil, A., Mohammed, F., Muhammed, E., Ramdane, H., Khalid, A.M., Mansour, A., Hassan, M., 2014. A hierarchical fuzzy control design for indoor mobile robot. *International Journal of Advanced Robotic Systems*. 1–16.
- Gadalla M., Zafar S., 2012. Analysis of a hydrogen fuel cell-PV power system for small UAV. *International journal of Hydrogen Energy*. 41 (2012) 6422-6432.
- Ge, H., 2010. Maintenance optimization for substations with aging equipment. University of Nebraska, Lincoln.

- Geem, Z.W., Kim, J.H., Loganathan, G.V., 2001. A new heuristic optimization algorithm: harmony search. *simulation*, 76(2), 60-68.
- Geng, N., Gong, D. W., Zhang, Y., 2014. PSO-based robot path planning for multisurvivor or rescue in limited survival time. *Mathematical Problems in Engineering*, 2014.
- Guo Z.Q., Wang H.Q., Liu Q., 2013. Financial time series forecasting using LPP and SVM optimized by PSO. *Soft Computing*, 17(5), 805-818.
- Han, S., Zhou, X., Chen, C., 2016. Path planning for multi-robot systems using PSO and Critical Path Schedule Method. In *Networking, Sensing, and Control (ICNSC)*, 2016 IEEE 13th International Conference on (pp. 1-6). IEEE.
- Hardware Engineer III in the United States, 2019. Available at: <https://www1.salary.com/Hardware-Engineer-III-hourly-wages.html>
- Hedelind, M., Jackson, M., 2011. How to improve the use of industrial robots in lean manufacturing systems. *Journal of Manufacturing Technology Management*. 22(7), 891-905.
- Herold, D.M., Farmer, S.M., Mobley, M.I., 1995. Pre-implementation attitudes toward the introduction of robots in a unionized environment. *Journal of Engineering and Technology Management*. 12(3), 155-173.
- Huang, S.H., Huang, Y.H., Blazquez, C.A. and Paredes-Belmar, G., 2018. Application of the ant colony optimization in the resolution of the bridge inspection routing problem. *Applied Soft Computing*, Volume 65.
- Islam, M. M., Zhong, X., Xiong, H.Y., Sun, Z.Y., 2018. Optimal scheduling of manufacturing and onsite generation systems in over-generation mitigation oriented electricity demand response program. *Computers & Industrial Engineering*, 115, 381-388.
- Janglova, D., 2004. Neural networks in mobile robot motion. *International Journal of Advanced Robotic Systems*. 15–22.
- Jiang, San, Wanshou Jiang, Wei Huang, Liang Yang. "UAV-based oblique photogrammetry for outdoor data acquisition and offsite visual inspection of transmission line." *Remote Sensing* 9, no. 3 (2017): 278.
- Jun, Z. B., 2014. Monocular Video Human Motion Tracking based on Hybrid PSO. *Journal of Multimedia*, 9(1).
- Kim T, Kwon S., 2012. Design and development of a fuel cell-powered small unmanned aircraft. *International journal of Hydrogen Energy* 37 (2012) 615-622.

- Laugier, C., Siegwart, R., 2008. Field and service robotics: results of the 6th international conference. *Berlin, Springer Science & Business Media*.
- Lee, J., Kwon, O., Zhang, L., Yoon, S.E., 2014. A selective retraction-based rrt planner for various environments. *IEEE Transactions on Robotics*. 1002–1011.
- Li Z.Y., Mu S.Y., et al., 2016. Transmission line intelligent inspection central control and mass data processing system and application based on UAV. *IEEE International Conference on Applied Robotics for the Power Industry*, 2016, pp. 1-5.
- Liu, H., Wan, W. and Zha, H., 2010. A dynamic subgoal path planner for unpredictable environments. *In Robotics and Automation (ICRA)*, 2010 IEEE International Conference on 994-1001.
- Mac, T.T., Copot, C., Tran, D.T. and De Keyser, R., 2016. Heuristic approaches in robot path planning: a survey. *Robotics and autonomous systems*. 86, 13-28.
- Mahmoudi, M., Barkany, A., Khalfi, A.E., 2014. A maintenance optimization policy for an electric power distribution system: case of the hv/mv substations. *Engineering*. 6, 236-253.
- Matrice 200 series. 2017. Available at: <https://www.dji.com/matrice-200-series/info#specs>
- Military grade monitor, 2018: (1) Available at: <http://www.acnodes.com/RM9230.htm> (2) Available at: <https://store.dji.com/product/crystalsky?vid=23531&from=pc-cart-title>
- MMC website: MMC HyDrone 1550 specific- Available at: <http://www.mmcuav.com/drones/hydrone1550/#spec> and MMC MMC Powerful Hydrogen H1-Fuel Cell- Available at: <http://www.mmcuav.com/wp-content/uploads/2017/02/H1-FuelCellBrochure.pdf>
- Montambault, S., Pouliot, N., 2003. The hq linerover: contributing to innovation in transmission line maintenance. *Proceedings of the 10th International Conference on Transmission and Distribution Construction and Live Line Maintenance (ESMO 2003)* 6-10 April 2013.
- Montambault, S., Pouliot, N., 2004. On the economic and strategic impact of robotics applied to transmission line maintenance. *Konferencja ICOLIM*.1-8.
- Montambault, S., Pouliot, N., 2012. Field-oriented developments for linescout technology and its deployment on large water crossing transmission lines. *Journal of Field Robotics*, 29(1), 25-46.

- Nagarajan B.R., Qin R.W., Sun Z.Y. Islam M.M., 2017. Cost Analysis For High Voltage Transmission Line Inspection Using Robot. *Proceedings of the American Society for Engineering Management* 2017.
- Onwunali, J. E., Durlofsky, L. J., 2010. Application of a particle swarm optimization algorithm for determining optimum well location and type. *Computational Geosciences*, 14(1), 183-198.
- Orr, S.C., 1996. A longitudinal survey of robot usage in australia. *Integrated Manufacturing Systems*. 7(5), 33-46.
- Pagell, M., Dibrell, C., Veltri, A., Maxwell, E., 2014. Is an efficacious operation a safe operation: the role of operational practices in worker safety outcomes. *IEEE transactions on engineering management*. 61(3), 511-521.
- Parh, D.R., Singh, M.K., 2009. Real-time navigational control of mobile robots using an artificial neural network. *Mechanical Engineering Science, Part C*. 1713–1725.
- Peri, V.M., Simon, D., 2005. Fuzzy logic control for an autonomous robot. *Annual Meeting of the North American Fuzzy Information Processing Society*. 337–342.
- Pradeepkumar, D., Ravi, V., 2017. Forecasting financial time series volatility using particle swarm optimization trained quantile regression neural network. *Applied Soft Computing*, 58, 35-52.
- Quanta Technology, LLC, 2015. Ground based robots & the future of applications of robots for transmission line work. Available at: <http://www.cce.umn.edu/documents/COPE-Conferences/MIPSYCON-PowerPoints/2015/DSIRobotsforEnergizedTransmissionLineWork.pdf>
- Roncolatto, R. A., Romanelli, N.W., CPFL-Paulista, Hirakawa, A., Horikawa, O., Vieira, D.M., Yamamoto, R., Finotto, V.C., Sverzuti, V., Lopes. I.P., 2010. Robotics applied to work conditions improvement in power distribution lines maintenance. Applied Robotics for the Power Industry (CARPI), *Proceedings of 2010 1st International Conference on Applied Robotics for the Power Industry*.
- Rosell, J. I., 2005. Path planning using harmonic functions and probabilistic cell decomposition. *International Conference on Robotics and Automation, ICRA*, 1803–1808. Barcelona, Spain.
- Saini, S., Zakaria, N., Rambli, D. R. A., Sulaiman, S., 2015. Markerless human motion tracking using hierarchical multi-swarm cooperative particle swarm optimization. *PLOS One*, 10(5), e0127833.

- Saravanan, M., Slochanal, S. M. R., Venkatesh, P., Abraham, J. P. S. 2007. Application of particle swarm optimization technique for optimal location of FACTS devices considering cost of installation and system loadability. *Electric Power Systems Research*, 77(3-4), 276-283.
- Šeda, M., 2007. Roadmap method vs. Cell decomposition in robot motion planning. *International Conference on Signal Processing, Robotics and Automation*. 127–132. Greece.
- Sharma, Y., Saini, S. C., Bhandhari, M., 2012. Comparison of dijkstra's shortest path algorithm with genetic algorithm for static and dynamic routing network. *International Journal of Electronics and Computer Science Engineering*. 1(2), 416-425.
- Shiau, J.K., Ma, D.M., Yang, P.Y., Wang, G.F. Gong, J.H., 2009. Design of a solar power management system for an experimental UAV. *IEEE transactions on aerospace and electronic systems*, 45(4), pp.1350-1360.
- Sim, S.K., Teo, M.Y., 1997. Enhancing flexibility of vision-based robots using an artificial neural network approach. *Integrated Manufacturing Systems*. 8(1), 43-49.
- Singh, N.N., Chatterjee, A., Chatterjee, A., Rakshit, A., 2011. A two-layered subgoal based mobile robot navigation algorithm with vision system and ir sensors. *Measurement*. 620-641.
- Sun, X., Wang, J., Wu, W., Liu, W., 2018. Genetic algorithm for optimizing routing design and fleet allocation of freeway service overlapping patrol. *Sustainability*. 10(11), 4120.
- Sun, Z.Y., Li, L., Dababneh, F., 2016. Plant-level electricity demand response for combined manufacturing system and heating, venting, and air-conditioning (HVAC) system. *Journal of cleaner production*, 135, pp.1650-1657.
- Sun, Z.Y., Dababneh, F., Li, L., 2018. Joint Energy, Maintenance, and Throughput Modeling for Sustainable Manufacturing Systems. *IEEE Transactions on Systems, Man, and Cybernetics: Systems*.
- TB55. 2018. Available at: https://www.amazon.com/DJI-Original-Intelligent-Battery-Matrice/dp/B0774ZW7L3/ref=sr_1_1?ie=UTF8&qid=1548350629&sr=8-1&keywords=DJI+TB55
- Tips for battery, 2018: Tips for battery charging and storage. Available at: <https://www.asus.com/support/FAQ/1009546/>
- Truck Driver - Heavy in the United States, 2019. Available at: <https://www1.salary.com/Truck-Driver-Heavy-hourly-wages.html>

- ULC Robotics, 2018. FAA compliant unmanned aerial inspection program for gas and electric utilities. Available at: <http://ulcrobotics.com/services/unmanned-aerial-utility-inspection-services/>
- Veziroğlu T. N., Şahin S., 2008. 21st Century's energy: Hydrogen energy system. *Energy Conversion and Management*, Volume 49, Issue 7, July 2008, Pages 1820-1831.
- Video recorder, 2018: Available at: <https://store.dji.com/product/zenmuse-x3-gimbal-camera?from=search-result-v2&position=0>
- Video generator, 2018: (1) Available at: https://megadepot.com/product/techniquip-dcg-200m-110-digital-video-generator-single-camera-input-110-vac-usa-power-supply?format=v&p=ms&source=ads&gclid=CjwKCAiAsoviBRAoEiwATm8OYP4Pcn2hie94tsQ3jT4fvQqne7Qc7NMDnAbEoE3YJW_AnAsbu2q2xoC3d0QAvD_BwE (2) Available at: https://www.adorama.com/lespg812.html?gclid=CjwKCAiAsoviBRAoEiwATm8OYK9dJdT_AUbo3kYZLh0fDIHoTnjmEwhZvkadi1atlh5mpArMXl14-RoCROwQAvD_BwE (3) Available at: https://www.adorama.com/krs6005.html?gclid=CjwKCAiAsoviBRAoEiwATm8OYImLmB4y5uuLQYG6Upd5rio6Y--ZDUmB96TKwjPBszvF4OGriQszvxoC0q4QAvD_BwE
- Wang B. H., Chen X.G., et al., 2010. Power line inspection with a flying robot. *International Conference on Applied Robotics for the Power Industry*. Ieee, Oct. 2010, pp. 1-6
- Wang B. H., Han L., et al., 2009. A flying robotic system for power line corridor inspection. *Proceedings of IEEE International Conference on Robotics and Biomimetics*. 2009, pp.2468-2473.
- Whitworth C. C., Duller A. W. G., Jones D.I. and Earp G.K., 2001. Aerial video inspection of overhead power lines. *Power Engineering Journal*, Vol.15, No.1, 2001, pp.25-32.
- Wilmeth, R. G., Usrey, M.W., 2000. Reliability-centered maintenance: a case study. *Engineering Management Journal*. 12(4), 25-31.
- Wireless UAV Data Link, 2018. Available at: https://www.amazon.com/SkyHopper-Wireless-Transmission-Enables-Telemetry/dp/B06XDCGBYP/ref=sr_1_1?ie=UTF8&qid=1548430971&sr=8-1&keywords=data+link+UAV
- Xu, J., Zeng, Y. and Zhang, R., 2017, December. UAV-enabled wireless power transfer: Trajectory design and energy region characterization. In *Globecom Workshops (GC Wkshps), 2017 IEEE* (pp. 1-7). IEEE.
- Yan G. J., Wang J. F., et al., 2007. An airborne multi-angle power line inspection system. *Proceedings of IEEE International Symposium on Geoscience and Remote Sensing*, 2007, pp.2913-2915.

- Yang J.C., 2009. A thermodynamic analysis of refueling of a hydrogen tank. *International Journal of Hydrogen Energy*. Volume 34, Issue 16, August 2009, Pages 6712-6721.
- Yang T. W., Yin H., et al. 2012. Overhead Power Line Detection from UAV Video Images. *IEEE International Conference on Mechatronics and Machine Vision in Practice*. 2012, pp. 74-79.
- Yao, F., Shao, G., Takaue, R., Tamaki, A., 2003. Automatic concrete tunnel inspection robot system. *Advanced Robotics Journal*. 17(4), 319-337.
- Yaqub, M., Sarkni, S., Mazzuchi, T., 2012. Feasibility analysis of solar photovoltaic commercial power generation in california. *Engineering Management Journal*. 24(4), 36-49.
- Zhang, Y., Yuan, X., Fang, Y. and Chen, S., 2017. UAV low altitude photogrammetry for power line inspection. *ISPRS International Journal of Geo-Information*, 6(1), p.14.
- Zhang, Y., Yuan, X., Li, W. Chen, S., 2017. Automatic Power Line Inspection Using UAV Images. *Remote Sensing*, 9(8), p.824.

VITA

Yu Li was born in Gansu, China. Yu received her bachelor's degree in engineering management from Yichun University, Jiangxi, China, in June 2012. She worked at Rider Levett Bucknall Limited Company as a Quantity Surveyor of electromechanical engineering from August 2012 to July 2017 in Beijing, China. She came to Missouri University of Science and Technology in August 2017 to pursue her master's degree in systems engineering. She joined the research team as a Graduate Research Assistant under the supervision of Dr. Zeyi Sun in January 2018 and worked on the project of "A Survey of Robotics Technology Used by Utility Companies for Costs Reduction" funded by Ameren. Based on the deliverables of this project, she published two papers. The first one titled "Routing Algorithm and Cost Analysis for Using Hydrogen Fuel Cell Powered Unmanned Aerial Vehicle in High-Voltage Transmission Line Inspection," was published in the proceedings of annual ASEM conference of 2018. The second one, titled "A Routing Algorithm for Inspecting Grid Transmission System Using Suspended Robot: Enhancing Cost-Effective and Energy Efficient Infrastructure Maintenance," was published by the Journal of Cleaner Production (Impact factor: 5.651). In May 2019, she received her MS degree in Systems Engineering from Missouri University of Science and Technology.